Transketolase of Staphylococcus aureus in the Control of Master Regulators of Stress Response During Infection

Xin Tan, Elodie Ramond, Anne Jamet, Jean-Philippe Barnier, Baptiste Decaux-Tramoni, Marion Dupuis, Daniel Euphrasie, Fabiola Tros, Ivan Nemazanyy, Jason Ziveri, et al.

Transketolase of *Staphylococcus aureus* is involved in the control of master regulators of stress response during infection

Xin Tan[1,2], Elodie Ramond[1,2], Anne Jamet[1,2], Jean-Philippe Barnier[1,2], Baptiste Decaux-Tramoni[1,2], Marion Dupuis[1,2], Daniel Euphrasie[1,2], Fabiola Tros[1,2], Ivan Nemazanyy[1,2,3], Jason Ziveri[1,2], Xavier Nassif[1,2], Alain Charbit[1,2] * and Mathieu Coureuil[1,2] *

[1] Université de Paris, Paris, France

[2] INSERM U1151 - CNRS UMR 8253, Institut Necker-Enfants Malades, Paris, France

[3] Plateforme Métabolomique Institut Necker, Structure Fédérative de Recherche SFR Necker, Université Paris Descartes, Paris 75015 France

Running title: Transketolase in *S. aureus* infection

Keywords: Transketolase, *Staphylococcus aureus*, metabolic adaptation, Pentose Phosphate Pathway, sigma B, RpiRc.

Abstract: 142 words; Text: 3315 words.

* Corresponding authors: Alain Charbit, Mathieu Coureuil

e-mail: alain.charbit@inserm.fr ; mathieu.coureuil@inserm.fr

Tel: 33 1 – 72 60 65 11 — Fax: 33 1 - 72 60 65 13

Conflict of interest: No potential conflict of interest was reported by the authors.

Funding: These studies were supported by INSERM, CNRS and Université Paris Descartes Paris Cité Sorbonne. This work was supported by Vaincre La Mucoviscidose (grant RF20180502254). Xin Tan was funded by a scholarship from the China Scholarship Council (n° CSC NO. 201508500097). The funders had no role in study design, data collection and analysis, decision to publish, or preparation of the manuscript.

Abstract

Staphylococcus aureus is a leading cause of both acute and chronic infections in humans. The importance of the pentose phosphate pathway (PPP) during *S. aureus* infection is currently largely unexplored. Here, we focused on one key PPP enzyme, transketolase. We showed that inactivation of the unique gene encoding transketolase activity in *S. aureus* USA300 (Δ*tkt*) led to drastic metabolomic changes. Using time-lapse video imaging and mice infection, we observed a major defect of the Δ*tkt* strain compared to wild-type strain in early intracellular proliferation and in the ability to colonise kidneys. Transcriptional activity of the two master regulators Sigma B and RpiRc was drastically reduced in the Δ*tkt* mutant during host cells invasion. The concomitant increased RNAIII transcription, suggests that TKT -or a functional PPP- strongly influences the ability of *S. aureus* to proliferate within host cells by modulating key transcriptional regulators.

Background

Staphylococcus aureus is a leading cause of severe skin and soft tissue infections, pneumonia, endocarditis and bone and joint infections [1, 2]. *S. aureus* invades and survives within eukaryotic host cells [3-9]. This is likely to play an important role in chronicity and treatment failures [10-12]. To evade host defences and silently persist within human cells [13, 14], *S. aureus* can dynamically switch phenotypes from a highly aggressive and cytotoxic phenotype to a metabolically inactive phenotype associated with decrease TCA activity [15-18]. Reprogramming of the TCA cycle notably involves the glycolysis/gluconeogenesis and pentose phosphate pathway (PPP) [19].

The contribution of glycolysis/gluconeogenesis to intracellular persistence of *S. aureus* has been recently studied [20-23]. In contrast, the precise role of the PPP is unexplored. The PPP is important for producing nucleotide precursors for DNA synthesis and repair as well as precursors for aromatic amino acids or peptidoglycan synthesis. In addition, the oxidative branch of the PPP contributes to bacterial tolerance to oxidative stress by generating the redox molecule $NADPH/H^+$, which is the substrate for other reducing agents such as glutathione. The activity of the PPP has been shown to be frequently increased in Gram-positive pathogens in response to environmental stresses and in infection models [24-26] or in some hospital-acquired isolates [27]. While it has been suggested that the transcriptional regulator RpiRc might control the PPP [28-30], no gene regulation has been yet associated with any change in its activity in *S. aureus.*

Here, we study the role of PPP during the intracellular persistence of *S. aureus* by focusing on one of the key enzyme of this pathway, transketolase (TKT). *tkt* genes are found in a wide range of organisms including bacteria, plants and mammals, underlining the ubiquitous role of this enzyme in biology. We show here that *tkt* inactivation in *S. aureus* USA300 leads to deregulation of whole cell metabolism. This correlates with impaired proliferation of intracellular staphylococci *in vitro* and kidney colonisation defect in infected mice. Unexpectedly, we found

that the *tkt* defective mutant was unable to regulate the two master regulators of virulence RpirC and SigB, leading to a dramatic increase of RNAIII during intracellular invasion of human cells. Altogether our data suggest a major role of the PPP in the control of *S. aureus* virulence.

Methods

Strains, Cells, Culture conditions and Infection.

S. aureus USA300-LAC (designated USA300-WT) was provided by the Biodefense and Emerging Infections Research Resources (BEI). The GFP-expressing strain, the Δ*tkt* mutant strain and the complemented strain were constructed and cultured as described in **supplementary methods**. Strains and plasmids used are summarized in **supplementary methods**.

S. aureus were grown in brain heart infusion (BHI) or chemically defined medium (CDM) supplemented with ribose or fructose or glycerol when it was required [31].

EA.hy926 endothelial cells (ATCC CRL-2922) were grown in DMEM 10 % FBS (5 % CO_2 at 37 °C). When indicated, cells were incubated with no glucose DMEM supplemented with glucose, ribose or fructose at a concentration of 25mM. EA.hy926 expressing nuclear mKate2 were transduced with the IncuCyte® NucLight Red Lentivirus.

Cells were infected at a multiplicity of infection (MOI) of 1 for 1 h and washed three times with 100 µL of phosphate buffer saline (PBS) containing 300 µg/ml gentamicin to remove extracellular bacteria. Cells were then incubated in PBS-gentamicin (50µg/ml). Gentamicin is an antibiotic with a high bactericidal effect on *S. aureus* USA300 (CMI=2 µg/ml) and a very poor penetration inside eukaryotic cells. Its use was necessary to abolish extracellular proliferation.

LAMP-1 colocalization assay in EA.hy926 infected cells is described in the **supplementary methods**.

Time lapse microscopy

EA.hy926 cells expressing nuclear mKate2 were seeded in ImageLock 96-well plates (Essen BioScience Inc). Cells were infected with WT and Δ*tkt* mutant of the GFP-expressing USA300 strain. Plates were incubated and monitored at 5% CO2 and 37°C for 24 hours in the fully automated microscope Incucyte® S3 (Essen BioScience). The detailed analysis is further described in the **supplementary methods**.

Transcriptional analyses

The bacteria were recovered from lysed cells or planktonic overnight culture. Nucleic acids were released by resuspending bacteria in TE buffer containing lysostaphin. RNAs recovery, reverse transcription and PCR were performed as described in the **supplementary methods**. We used the “The Relative Standard Curve Method” for analyzing the qRT-PCR data.

Metabolomic analyses

Metabolite profiling of *S. aureus* isolates grown to stationary phase in BHI Broth was performed by liquid chromatography–mass spectrometry (LC-MS) as described in the **supplementary methods** [9, 32, 33].

Transketolase activity assay

TKT activity was analysed on bacteria grown to stationary phase in BHI as described in the **supplementary methods** [34]. TKT activity was expressed as units per microgram of total protein. One unit of enzyme was defined as the amount of enzyme that oxidized 1 µmol of NADH per minute.

***In vivo* infection**

Mice were infected intravenously (iv) in the tail vein as described in the **supplementary methods**. For bacterial burden determination, mice were euthanized after 4, 24, 48 and 72 hours. Sequential dilutions of homogenized preparations from spleen and kidney were spread onto BHI agar plates.

Statistics

Statistical significances were assessed using one-way analysis of variance (ANOVA) with Dunnett’s correction, unpaired two-tail Student’s t-test, or Kruskal Wallis test. P values of $p<0.05$ were considered to indicate statistical significance.

Ethics statement

All experimental procedures involving animals were conducted in accordance with guidelines established by the French and European regulations for the care and use of laboratory animals (Decree 87–848, 2001–464, 2001–486 and 2001–131 and European Directive 2010/63/UE) and approved by the INSERM Ethics Committee (Authorization Number: 75-906).

Results

196

197 **Transketolase inactivation in *S. aureus* USA300**

198 *S. aureus* genomes possess a unique transketolase-encoding gene, designated *tkt,*
199 which is highly conserved within species. Transketolase (TKT) is an enzyme of the non-
200 oxidative branch of the PPP involved in two main reversible enzymatic reactions: i) Fructose-
201 6-P + Glyceraldehyde-3-P <-> Erythrose-4-P + Xylulose-5-P; and ii) Sedoheptulose-7-P +
202 Glyceraldehyde-3-P <-> Ribose-5-P + Xylulose-5-P (**Supplementary Figure S2A)**. Several
203 TKT structures have been solved [35] and allow the modelisation of the *S. aureus* TKT
204 **(Supplementary Figure S1B).** The protein of *S. aureus* is 662 amino acid long and harbours
205 three domains **(Supplementary Figure S1A)**. Of note, although ubiquitously expressed in
206 Eukaryotes and Bacteria, *S. aureus* and *Homo sapiens* TKT proteins share only 22.4% amino
207 acid identity **(Supplementary Figure S1C)**. We constructed a chromosomal deletion of the *tkt*
208 gene in *S. aureus* strain USA300 (Δ*tkt* strain), and generated a complemented strain
209 (designated Cp-*tkt*) by expressing the wild-type *tkt* allele preceded by its own promoter in the
210 Δ*tkt* strain. Gene inactivation was confirmed by quantification of the transketolase activity
211 (**Supplementary Figure S2)**.

212 The Δ*tkt* mutant showed only a slight growth decrease compared to the WT strain in
213 complete BHI Broth or in Dulbecco's Modified Eagle Medium (DMEM) (**Figure 1A**). In contrast,
214 the Δ*tkt* mutant strain was unable to grow in chemically defined medium [31] supplemented
215 with ribose (which can be converted to Ribose-5-phospate by ribokinase) (**Supplementary**
216 **Figure S2C**). In all assays, functional complementation was observed in the Cp-*tkt* strain.

217 We next performed a whole cell metabolomic analysis on WT and Δ*tkt* strains grown for
218 24h in BHI Broth (*i.e.,* when identical numbers of cells were recorded) to evaluate the global
219 impact of *tkt* deletion on bacterial metabolism (**Figure 1B and Supplementary Figure S3 and**
220 **Table S1**). Remarkably, we observed a massive accumulation of ribose-5-phosphate (R5P;
221 56-fold increase) concomitant with a decrease in ribose content (4-fold decrease) in the Δ*tkt*
222 mutant compared to WT. This accumulation was associated with an increased amount of
223 metabolites derived from Ribose-5P, such as inosine-5-monophosphate (IMP), xanthosine-5-
224 monophosphate (XMP) and hypoxanthine. We also observed a 2.5-fold decrease in D-sedo-

heptulose-7P amount in the Δ*tkt* mutant compared to WT accompanied by a significant decrease in tyrosine, histidine and tryptophan amounts (5, 10 and 12 fold respectively), three aromatic amino-acids produced from the PPP. The glutamate pathway seemed to be significantly more active in the Δ*tkt* strain compared to WT as the amounts of glutamate, proline and ornithine were all increased. The higher amounts of glutamate, possibly fuelling the TCA cycle at the level of α-ketoglutarate, could be responsible for the increased expression of some TCA cycle metabolites (*i.e.,* fumarate, malate, succinate and α-ketoglutarate) in the Δ*tkt* strain. Of note, ATP content was not altered in Δ*tkt* strain. These results demonstrate that deregulation of the PPP by *tkt* inactivation has direct effects on the whole cell metabolism, including aromatic amino acid production, TCA activity and pathways involved in adenine, guanine or peptidoglycan synthesis.

Tkt is essential for intracellular proliferation of _S. aureus_

Intracellular staphylococci exist as two different populations: bacteria that actively proliferate during the first 24 hrs after invasion, leading to their release in extracellular milieu as a consequence of host cell death, and bacteria that do not replicate. These latter staphylococci can persist within host-cell cytoplasm for several days [3-9, 36]. Here we addressed the role of TKT in these two phenotypes in EA.hy926 human endothelial cells by using: i) time lapse-microscopy, to evaluate early intracellular proliferation of *S. aureus* and ii) colony forming units counting, to monitor the survival kinetics of internalized bacteria over a ten days period.

Time-lapse video microscopy. EA.hy926 cells expressing mKate2 nuclear fluorescent protein were infected by GFP-expressing bacteria. Gentamicin was used throughout the experiment to eliminate extracellular bacteria and prevent re-infection (see Methods), allowing us to solely focus on the fate of intracellular persistent bacteria. Cell infection was monitored using an IncuCyte® S3 imaging system and images were captured every 30 minutes. Bacterial entry into endothelial cells was similar for WT and Δ*tkt* strains, showing 0.3~0.5 GFP expressing particles recorded per cell (**Figure 2A-B**). Active proliferation of WT *S. aureus* inside EA.hy926 cells was confirmed after 24 hours of infection (**Figure 2A-B and Movie 1)**

with an average number of GFP expressing particles rising from 0.5 to 2 per cells. At the single cell level, WT *S. aureus* showed active intracellular multiplication, ultimately leading to cell death and bacterial release in the extracellular medium (**Figure 2A-B and Movie 1**). Thanks to the permanent presence of gentamicin in the medium bacterial release did not lead to proliferation in the extracellular medium. In contrast, the Δ*tkt* mutant strain showed limited proliferation during the first 24 hours (**Figure 2A-B and Movie 2**). Finally, using LAMP-1 colocalization assay (Lysosome-associated membrane protein 1), we confirmed that the intracellular Δ*tkt* strain growth defect was not due to a decreased phagosomal escape (**Supplementary Figure S4**).

Long-term intracellular survival. Using the same infection conditions as for time-lapse experiment, we monitored survival of internalised Δ*tkt* mutant compared to that of the WT strain at three, seven or ten days after infection by CFU counting. The Δ*tkt* strain behaved likes the WT strain throughout the infection period, ultimately leading to its complete elimination after 10 days (**Figure 2C**).

Thus, the role of TKT during *S. aureus* host cell infection seems to be essential for bacteria proliferation and restricted to early time points.

Tkt inactivation is associated with an altered _rpiRc_ and _sigB_ expression.

S. aureus is known to sense its environment and to regulate virulence factors depending on the availability of carbon sources. For example, recent studies have shown that the transcriptional regulator RpiRc could sense metabolic shifts, especially in the PPP, and control expression of RNAIII [29, 30]. RNAIII is a key effector in the quorum-sensing system that regulates the expression of a large number of virulence factors [37]. RpiRc is also linked to the alternative Sigma B factor (SigB) that has pleiotropic roles in gene regulation and is a master regulator of intracellular survival [29, 38, 39].

These data prompted us to follow the expression profile of the master regulator SigB and RpiRc in the WT and the Δ*tkt* mutant strains during endothelial cells invasion (**Figure 3**). EA.hy296 cells were infected as described above to solely focus on intracellular bacteria. Between day 1 and day 7, *sigB* and *rpiRc* transcription increased in the WT strain (by 4-fold

and 3-fold, respectively) (**Figure 3**). In sharp contrast, as early as one day after infection, both genes were significantly down-regulated in the Δ*tkt* mutant strain compared to WT (8-fold and 7-fold decrease for *sigB* and *rpirC* expression, respectively). Consistent with reports demonstrating inhibition of RNAIII expression by RpirC and SigB [18], we observed a dramatic increase in the expression of *RNAIII* in the Δ*tkt* mutant strain (**Figure 3**), suggesting that the Δ*tkt* mutant strain is unable to control *rpiRc* and *sigB* expression during intracellular survival. Functional complementation always restored the wild type phenotype (**Supplementary Figure S5**). To further confirm these data, we monitored the expression of two major regulators of SigB activity, RsbU and RsbW [40]. RsbW, which is co-expressed with *sigB*, is known to sequestrate and inhibit SigB. RsbU, whose expression is under the control of SigA, is a phosphatase involved in the dephosphorylation of RsbV. In turn, dephosphorylated RsbV (dRsbV) is able to sequestrate RsbW, allowing the release of active SigB. RsbU is thus considered as an activator of SigB, allowing a fine-tuning of SigB activity.

We found that the transcription of both *rsbW* and *rsbU* genes was down-regulated in the Δ*tkt* mutant during infection of endothelial cells. The down-regulation of *rsbW* is consistent with the down-regulation of its co-expressed gene *sigB* (**Figure 3**). The concomitant down-regulation of *rsbU* suggests a global inhibition of the *sigB* pathway in the Δ*tkt* mutant strain. Finally, we followed expression of *asp23*, a *sigB*-dependent locus [41]. The recorded down-regulation of *asp23* transcription in the Δ*tkt* mutant strain confirmed the inhibition of SigB-dependent transcription. All together these transcriptional analyses suggest that the metabolic deregulation observed in Δ*tkt* strain is sufficient to promote a dramatic reprogramming of the RpiRc and SigB pathways when bacteria invade human cells.

Tkt **inactivation impairs proliferation of *S. aureus* in the kidney of infected mice.**

The ability of internalized *S. aureus* to readily proliferate inside host cell cytoplasm may be seen as an effective mechanism to avoid host innate immunity, ultimately allowing an increased colonization of the infected site. In this respect, it has been previously shown in the mouse model that after intravenous (IV) injection, although rapidly cleared from the

bloodstream, bacteria were able to proliferate in the kidney, leading to abscesses formation within the first days of infection [42].

Here, we monitored the kinetics of *in vivo* proliferation of WT, Δ*tkt* and Cp-*tkt* strains in kidneys and spleens of BalB/c mice (**Figure 4**) after IV infection with 10^7 bacteria per mouse. As previously reported, *S. aureus* poorly proliferates in the spleen of infected mice. We therefore used the spleen as a non proliferative control. The bacterial burden in kidneys and spleens was quantified by plating CFUs at 4 h, 24 h, 48 h and 72 h after infection. We observed no significant differences between the bacterial counts in the spleens of mice infected either with WT, the *Δtkt* mutant or the Cp-*tkt* strain. In each case, a progressive reduction of the bacterial burden was recorded (ranging from $2.5x10^5$, $1.1x10^5$ and $1.5x10^5$ at 4 h; down to $3x10^3$, $7.3x10^2$ and $1.2x10^2$ at 72 h, for WT, Δ*tkt* and Cp-*tkt* respectively). In contrast, in kidneys, whereas the WT and the Cp-*tkt* strains readily proliferated (from $3.9x10^4 \pm 8.6x10^3$ WT and $2.1x10^4 \pm 4.6x10^2$ Cp-*tkt S. aureus* per organ at 4 hrs to $7.7x10^7 \pm 3.3x10^7$ WT and $3.6x10^7 \pm 1.3x10^7$ Cp-*tkt S. aureus* per organ at 72 hrs), multiplication of the Δ*tkt* mutant was severely impaired at all time-points tested, with a 10^4-fold reduction of Δ*tkt* counts at 24h compared to WT counts (**Figure 4**). This result confirms the importance of TKT -and most likely of the PPP- in bacterial proliferation *in vivo* and especially during the first 24 hours after infection. This result is consistent with the previously described role of SigB in intracellular growth *in vivo* [43].

The SigB pathway may be controlled by modulating carbon source availability.

Inside the cytoplasm of host cells, the Δ*tkt* mutant is likely to deal simultaneously with PPP blocking and altered levels of carbon-based nutrients compared to the outside compartment. The above results suggested that the PPP might take control of *rpiRc* and *sigB* expression when bacteria invade endothelial cells. We thus hypothesized that PPP-associated carbon sources may possibly influence *rpiRc* and/or *sigB* expression *in vitro*. We therefore grew WT USA300 in CDM supplemented either with glucose (CDM-glucose), ribose (CDM-ribose) or fructose (CDM-fructose) a carbon source possibly fuelling the PPP) and quantified by qRT-PCR the transcription of *sigB*, *rpiRc*, *rsbU/W* and *asp23* genes. Remarkably, we found that the regulation of the whole *sigB* operon was impacted by the carbon source used in CDM

(**Figure 5**). Indeed, expression of *sigB, rsbU/W* and *rpiRc* decreased in CDM-fructose or CDM-ribose, compared to CDM-glucose. In contrast, *asp23* expression was only decreased by 2-fold in CDM-fructose and increased by 3-fold in CDM-ribose, suggesting that in this growth conditions, *asp23* expression might be regulated by other factor than *sigB* (**Figure 5**). Hence, the availability of carbon sources, and especially those related to PPP, may be sensed by the bacteria and affect the regulation of *rpiRc* and *sigB* expression.

Discussion

Inactivation of the *tkt* gene, encoding the unique transketolase of *S. aureus* USA300, led to a major decrease in early intracellular proliferation and impaired *in vivo* the multiplication

in a kidney colonization model. Our results suggest that the intracellular proliferation defect of the Δ*tkt* mutant occurs through the inhibition of *sigB* and *rpiRc* expression and the concomitant increased *RNAIII* transcription, thus highlighting a novel connection between the PPP and these master regulators during cell invasion.

Our whole cell metabolomic analysis of planktonic-grown bacteria (**Figure 1, Supplementary Figure S2 and Table S1**) showed a huge increase in R5P intermediates in the Δ*tkt* mutant compared to WT that could be explained by the impaired entry of R5P into glycolysis and a concomitant significant decrease in SH7P relative concentration. In *S. aureus*, ribose is imported by the RbsU transporter and converted to R5P by the RbsD/RbsK pathway. RbsR, the repressor of *rbsUDK* operon, is itself highly regulated by SigB [44]. Interestingly, *S. aureus* grown in CDM-ribose showed a decreased expression of *sigB*. Hence, stress signals that modulate SigB activity are likely to be important effectors for controlling the quantity of RbsR, thereby affecting ribose uptake.

Significant changes in the relative concentrations of TCA cycle intermediates were also recorded in the Δ*tkt* mutant compared to WT (**Supplementary Figure S3**). The TCA cycle plays a central role in maintaining the bacterial metabolic status and has been repeatedly implicated in the regulation of staphylococcal virulence [45, 46]. Hence, changes in TCA cycle activity are likely to induce alterations of the overall metabolome of the bacterium that, in turn, may modulate the activity of metabolite-responsive global regulators such as SigB or RpiR.

RpiRc, a RpiR family-member controlling enzymes involved in sugar catabolism in *S. aureus*, has been shown to repress RNAIII [28], supporting the notion of a direct connection between the PPP and the regulation of *S. aureus* virulence. The expression of *sigB* has also been shown to play a crucial role during the intracellular life of bacteria possibly by down-regulating pro-inflammatory virulence factors and increasing the expression of factors promoting persistence [18, 39].

We propose (**Figure 6**) that in wild-type *S. aureus*, transketolase activity results in a positive regulation of *rpiRc* and *sigB* transcription and allows the repression of RNAIII. Consequently, repression of toxins production favours intracellular growth. In contrast, in a Δ*tkt* mutant, *rpiRc* and *sigB* transcriptions are not activated, possibly due to metabolic changes

398 (such as R5P accumulation) and RNAIII is not repressed. At this stage, it cannot be excluded
399 that the enzyme itself might also directly affect transcription of these regulators.
400 TKT inhibitors are currently actively tested in cancer therapy [47] and TKT could
401 constitute an efficient target against tuberculosis [35] and malaria [48]. The present work,
402 highlighting an unprecedentedly reported role of transketolase in *S. aureus* intracellular
403 survival, suggests that modulation of the pentose phosphate pathway activity may also
404 represent an interesting mean to fight *S. aureus* infections.
405

Legends

Figure 1. Phenotypic characterization of the Δ*tkt* mutant

A. Growth of USA300 wild type (WT), Δ*tkt* mutant (Δ*tkt*) and its complemented derivative (Cp-*tkt*). USA300 WT, Δ*tkt* and Cp-*tkt* strains were grown in BHI Broth or DMEM for 21 hours at 37°C. Optic densities were measured every hour from 0 to 8 hours and then at 21 hours. Each panel is a representative experiment.

B. Metabolomic analysis of the Δ*tkt* mutant strain. Quantitative metabolomic analysis was performed by ion chromatography and tandem mass spectrometry (IC-MS/MS) after overnight cultures, in BHI Broth, from WT USA300 and Δ*tkt* mutant strains (see **Table S1**). The heatmap, obtained using MetaboAnalyst (https://www.metaboanalyst.ca), illustrates the metabolic shift between the two strains.

Figure 2. Intracellular proliferation and persistence of *S. aureus*.

A, B. Intracellular proliferation of USA300 wild type (WT) and Δ*tkt* mutant (Δ*tkt*) strains. Endothelial EA.hy926 cells expressing mKate2 nuclear restricted red fluorescent protein were infected with GFP expressing WT and Δ*tkt* strains. One hour after infection, cells were washed several times with gentamicin containing medium to eliminate extracellular bacteria. Gentamicin concentration of 50µg/ml was maintained throughout the experiment. Images were acquired every 30 minutes using Incucyte® S3 live cell imaging system. A. Representative images (see also Movie 1 and 2). Red: cell nuclei. Green: GFP expressing bacteria. For each line, a white circle was centred on a unique infected cell. Bar = 100µm. B. Quantitative analysis representing the number of green particles divided by the number of red nuclei during the first day after infection. Blue line: WT strain. Red line: Δ*tkt* strain. Black line: non infected cells.

C. Persistence of intracellular WT and Δ*tkt* strains. Endothelial EA.hy926 cells were infected with WT and Δ*tkt* strains as described above. Gentamicin was maintained throughout the experiment. Survival of *S. aureus* was assessed by plating and counting CFUs three, seven and ten days after infection. Results are shown as mean ± SD of triplicate measurements.

Figure 3. Transcription profile of intracellular *S. aureus*.

Endothelial EA.hy926 cells were infected with USA300 WT and Δ*tkt* strain as described in figure 2. One, three or seven days after infection, cells were washed and collected. RNA from intracellular *S. aureus* were prepared and gene expression of *RNAIII*, *rpiRc*, *sigB*, *rsbU, rsbW* and *asp23* was analysed by quantitative RT-PCR. Gene expression level was normalized by that of *gyrA* at days 1, 3 and 7 after infection of EA-hy296 cells. Data are shown as mean normalized expression ± SD of triplicate measurements from two independent experiments. (ANOVA, ns: not statistically different; * $p<0.01$, ** $p<0.001$). Functional complementation was assessed on two other independent experiments and presented in **Supplementary Figure S5**.

Figure 4. Proliferation of *S. aureus* in the spleen and the kidney of infected mice.

Bacterial loads in the spleen and the kidney of BalB/c mice infected intravenously with 10^7 bacteria of the WT, Δ*tkt* and Cp-*tkt* strain. Bacterial counts are expressed in CFU/organ (WT and Δ*tkt* n=10; Cp-*tkt* n=6). Data are shown as mean ± SD. Statistical significance was determined using the Kruskal Wallis test with Dunn's correction (ns: not statistically different, *** $p<0.001$, **** $p<0.0001$). No statistical significance between strains was observed in the spleen of infected mice.

Figure 5. Carbon sources influence the transcription profile of the SigB pathway.

S. aureus USA300 WT strain was grown to stationary phase in CDM supplemented with glucose or ribose or fructose and gene expression profile of *rpiRc*, *sigB*, *rsbU, rsbW* and *asp23* was analysed by quantitative RT-PCR. Gene expression level was normalized by that of *gyrA*. Data are shown as mean normalized expression ± SD of triplicate measurements from two independent experiments. Statistical significance was assessed in comparison to bacteria grown in CDM glucose (ANOVA, * $p<0.01$, ** $p<0.001$).

Figure 6. Schematic depiction of the impact of TKT inactivation on *sigB* and *rpiRc* regulation.

SigB dependent regulation of *RNAIII* in *Δtkt* context.

Movie 1: Intracellular proliferation of USA300 wild type strain. Endothelial EA.hy926 cells expressing a nuclear restricted Red Fluorescent Protein were infected with GFP expressing wild type strains. One hour after infection cells were washed several times with gentamicin containing medium to eliminate extracellular bacteria (see materials and methods section). Gentamicin concentration of 50µg/ml was maintained throughout the experiment. Images were acquired every 30 minutes using Incucyte® S3 live cell imaging system.

Movie 2: Intracellular proliferation of USA300 Δ*tkt* mutant strain. Same protocol as above in movie 1.

Acknowledgements

We are grateful to the Cell imaging core facility of the "Structure Fédérative de Recherche" Necker INSERM US24/CNRS UMS3633 for his technical support.

The following reagents were provided by the Network on Antimicrobial Resistance in *Staphylococcus aureus* (NARSA) for distribution by BEI Resources, NIAID, NIH: *Staphylococcus aureus*, Strain USA300-0114, NR-46070; *Escherichia coli – Staphylococcus aureus* Shuttle Vector pNR-46158, Recombinant in *Staphylococcus aureus*, NR-46158.

References

1. Otto M. Community-associated MRSA: what makes them special? Int J Med Microbiol **2013**; 303:324-30.

493 2. Thomer L, Schneewind O, Missiakas D. Pathogenesis of Staphylococcus aureus
494 Bloodstream Infections. Annual review of pathology **2016**; 11:343-64.
495 3. Proctor RA, von Eiff C, Kahl BC, et al. Small colony variants: a pathogenic form of bacteria
496 that facilitates persistent and recurrent infections. Nature reviews Microbiology **2006**; 4:295-
497 305.
498 4. Tuchscherr L, Heitmann V, Hussain M, et al. Staphylococcus aureus small-colony variants
499 are adapted phenotypes for intracellular persistence. The Journal of infectious diseases **2010**;
500 202:1031-40.
501 5. Strobel M, Pfortner H, Tuchscherr L, et al. Post-invasion events after infection with
502 Staphylococcus aureus are strongly dependent on both the host cell type and the infecting S.
503 aureus strain. Clin Microbiol Infect **2016**; 22:799-809.
504 6. Hayes SM, Howlin R, Johnston DA, et al. Intracellular residency of Staphylococcus aureus
505 within mast cells in nasal polyps: A novel observation. The Journal of allergy and clinical
506 immunology **2015**; 135:1648-51.
507 7. Hanssen AM, Kindlund B, Stenklev NC, et al. Localization of Staphylococcus aureus in
508 tissue from the nasal vestibule in healthy carriers. BMC microbiology **2017**; 17:89.
509 8. Moldovan A, Fraunholz MJ. In or out: phagosomal escape of Staphylococcus aureus.
510 Cellular microbiology **2018**:e12997.
511 9. Tan X, Coureuil M, Ramond E, et al. Chronic Staphylococcus aureus lung infection
512 correlates with proteogenomic and metabolic adaptations leading to an increased intracellular
513 persistence. Clin Infect Dis **2019**.
514 10. Branger C, Gardye C, Lambert-Zechovsky N. Persistence of Staphylococcus aureus
515 strains among cystic fibrosis patients over extended periods of time. J Med Microbiol **1996**;
516 45:294-301.
517 11. Kahl BC, Duebbers A, Lubritz G, et al. Population dynamics of persistent Staphylococcus
518 aureus isolated from the airways of cystic fibrosis patients during a 6-year prospective study.
519 Journal of clinical microbiology **2003**; 41:4424-7.
520 12. Fisher RA, Gollan B, Helaine S. Persistent bacterial infections and persister cells. Nature
521 reviews Microbiology **2017**; 15:453-64.

522 13. Grosz M, Kolter J, Paprotka K, et al. Cytoplasmic replication of Staphylococcus aureus
523 upon phagosomal escape triggered by phenol-soluble modulin alpha. Cellular microbiology
524 **2014**; 16:451-65.
525 14. Korea CG, Balsamo G, Pezzicoli A, et al. Staphylococcal Esx proteins modulate apoptosis
526 and release of intracellular Staphylococcus aureus during infection in epithelial cells. Infection
527 and immunity **2014**; 82:4144-53.
528 15. Kohler C, von Eiff C, Liebeke M, et al. A defect in menadione biosynthesis induces global
529 changes in gene expression in Staphylococcus aureus. Journal of bacteriology **2008**;
530 190:6351-64.
531 16. Kriegeskorte A, Konig S, Sander G, et al. Small colony variants of Staphylococcus aureus
532 reveal distinct protein profiles. Proteomics **2011**; 11:2476-90.
533 17. Kriegeskorte A, Grubmuller S, Huber C, et al. Staphylococcus aureus small colony variants
534 show common metabolic features in central metabolism irrespective of the underlying
535 auxotrophism. Frontiers in cellular and infection microbiology **2014**; 4:141.
536 18. Tuchscherr L, Loffler B. Staphylococcus aureus dynamically adapts global regulators and
537 virulence factor expression in the course from acute to chronic infection. Current genetics
538 **2016**; 62:15-7.
539 19. Stincone A, Prigione A, Cramer T, et al. The return of metabolism: biochemistry and
540 physiology of the pentose phosphate pathway. Biological reviews of the Cambridge
541 Philosophical Society **2015**; 90:927-63.
542 20. Harper L, Balasubramanian D, Ohneck EA, et al. Staphylococcus aureus Responds to the
543 Central Metabolite Pyruvate To Regulate Virulence. mBio **2018**; 9.
544 21. Purves J, Cockayne A, Moody PC, Morrissey JA. Comparison of the regulation, metabolic
545 functions, and roles in virulence of the glyceraldehyde-3-phosphate dehydrogenase
546 homologues gapA and gapB in Staphylococcus aureus. Infection and immunity **2010**; 78:5223-
547 32.
548 22. Vitko NP, Spahich NA, Richardson AR. Glycolytic dependency of high-level nitric oxide
549 resistance and virulence in Staphylococcus aureus. mBio **2015**; 6.

550 23. Vitko NP, Grosser MR, Khatri D, Lance TR, Richardson AR. Expanded Glucose Import
551 Capability Affords Staphylococcus aureus Optimized Glycolytic Flux during Infection. mBio
552 **2016**; 7.
553 24. Gardner SG, Marshall DD, Daum RS, Powers R, Somerville GA. Metabolic Mitigation of
554 Staphylococcus aureus Vancomycin Intermediate-Level Susceptibility. Antimicrobial agents
555 and chemotherapy **2018**; 62.
556 25. Fleury B, Kelley WL, Lew D, Gotz F, Proctor RA, Vaudaux P. Transcriptomic and metabolic
557 responses of Staphylococcus aureus exposed to supra-physiological temperatures. BMC
558 microbiology **2009**; 9:76.
559 26. Joseph B, Schneiker-Bekel S, Schramm-Gluck A, et al. Comparative genome biology of a
560 serogroup B carriage and disease strain supports a polygenic nature of meningococcal
561 virulence. Journal of bacteriology **2010**; 192:5363-77.
562 27. Mekonnen SA, Palma Medina LM, Michalik S, et al. Metabolic niche adaptation of
563 community- and hospital-associated methicillin-resistant Staphylococcus aureus. Journal of
564 proteomics **2018**.
565 28. Zhu Y, Nandakumar R, Sadykov MR, et al. RpiR homologues may link Staphylococcus
566 aureus RNAIII synthesis and pentose phosphate pathway regulation. Journal of bacteriology
567 **2011**; 193:6187-96.
568 29. Gaupp R, Wirf J, Wonnenberg B, et al. RpiRc Is a Pleiotropic Effector of Virulence
569 Determinant Synthesis and Attenuates Pathogenicity in Staphylococcus aureus. Infection and
570 immunity **2016**; 84:2031-41.
571 30. Balasubramanian D, Ohneck EA, Chapman J, et al. Staphylococcus aureus Coordinates
572 Leukocidin Expression and Pathogenesis by Sensing Metabolic Fluxes via RpiRc. mBio **2016**;
573 7.
574 31. Hussain M, Hastings JG, White PJ. A chemically defined medium for slime production by
575 coagulase-negative staphylococci. J Med Microbiol **1991**; 34:143-7.
576 32. Mackay GM, Zheng L, van den Broek NJ, Gottlieb E. Analysis of Cell Metabolism Using
577 LC-MS and Isotope Tracers. Methods in enzymology **2015**; 561:171-96.

578 33. Chong J, Soufan O, Li C, et al. MetaboAnalyst 4.0: towards more transparent and
579 integrative metabolomics analysis. Nucleic acids research **2018**; 46:W486-W94.
580 34. Shaw JA, Henard CA, Liu L, Dieckman LM, Vazquez-Torres A, Bourret TJ. Salmonella
581 enterica serovar Typhimurium has three transketolase enzymes contributing to the pentose
582 phosphate pathway. The Journal of biological chemistry **2018**; 293:11271-82.
583 35. Fullam E, Pojer F, Bergfors T, Jones TA, Cole ST. Structure and function of the
584 transketolase from Mycobacterium tuberculosis and comparison with the human enzyme.
585 Open biology **2012**; 2:110026.
586 36. Rollin G, Tan X, Tros F, et al. Intracellular Survival of Staphylococcus aureus in Endothelial
587 Cells: A Matter of Growth or Persistence. Frontiers in microbiology **2017**; 8:1354.
588 37. Boisset S, Geissmann T, Huntzinger E, et al. Staphylococcus aureus RNAIII coordinately
589 represses the synthesis of virulence factors and the transcription regulator Rot by an antisense
590 mechanism. Genes & development **2007**; 21:1353-66.
591 38. Mader U, Nicolas P, Depke M, et al. Staphylococcus aureus Transcriptome Architecture:
592 From Laboratory to Infection-Mimicking Conditions. PLoS genetics **2016**; 12:e1005962.
593 39. Tuchscherr L, Bischoff M, Lattar SM, et al. Sigma Factor SigB Is Crucial to Mediate
594 Staphylococcus aureus Adaptation during Chronic Infections. PLoS pathogens **2015**;
595 11:e1004870.
596 40. Pane-Farre J, Jonas B, Hardwick SW, et al. Role of RsbU in controlling SigB activity in
597 Staphylococcus aureus following alkaline stress. Journal of bacteriology **2009**; 191:2561-73.
598 41. Gertz S, Engelmann S, Schmid R, Ohlsen K, Hacker J, Hecker M. Regulation of sigmaB-
599 dependent transcription of sigB and asp23 in two different Staphylococcus aureus strains.
600 Molecular & general genetics : MGG **1999**; 261:558-66.
601 42. Cheng AG, Kim HK, Burts ML, Krausz T, Schneewind O, Missiakas DM. Genetic
602 requirements for Staphylococcus aureus abscess formation and persistence in host tissues.
603 Faseb J **2009**; 23:3393-404.
604 43. Tuchscherr L, Geraci J, Loffler B. Staphylococcus aureus Regulator Sigma B is Important
605 to Develop Chronic Infections in Hematogenous Murine Osteomyelitis Model. Pathogens
606 **2017**; 6.

607 44. Lei MG, Lee CY. RbsR Activates Capsule but Represses the rbsUDK Operon in
608 Staphylococcus aureus. Journal of bacteriology **2015**; 197:3666-75.
609 45. Somerville GA, Cockayne A, Durr M, Peschel A, Otto M, Musser JM. Synthesis and
610 deformylation of Staphylococcus aureus delta-toxin are linked to tricarboxylic acid cycle activity.
611 Journal of bacteriology **2003**; 185:6686-94.
612 46. Ding Y, Liu X, Chen F, et al. Metabolic sensor governing bacterial virulence in
613 Staphylococcus aureus. Proceedings of the National Academy of Sciences of the United
614 States of America **2014**; 111:E4981-90.
615 47. Xu IM, Lai RK, Lin SH, et al. Transketolase counteracts oxidative stress to drive cancer
616 development. Proceedings of the National Academy of Sciences of the United States of
617 America **2016**; 113:E725-34.
618 48. Thota S, Yerra R. Drug Discovery and Development of Antimalarial Agents: Recent
619 Advances. Current protein & peptide science **2016**; 17:275-9.
620
621

Figure 1

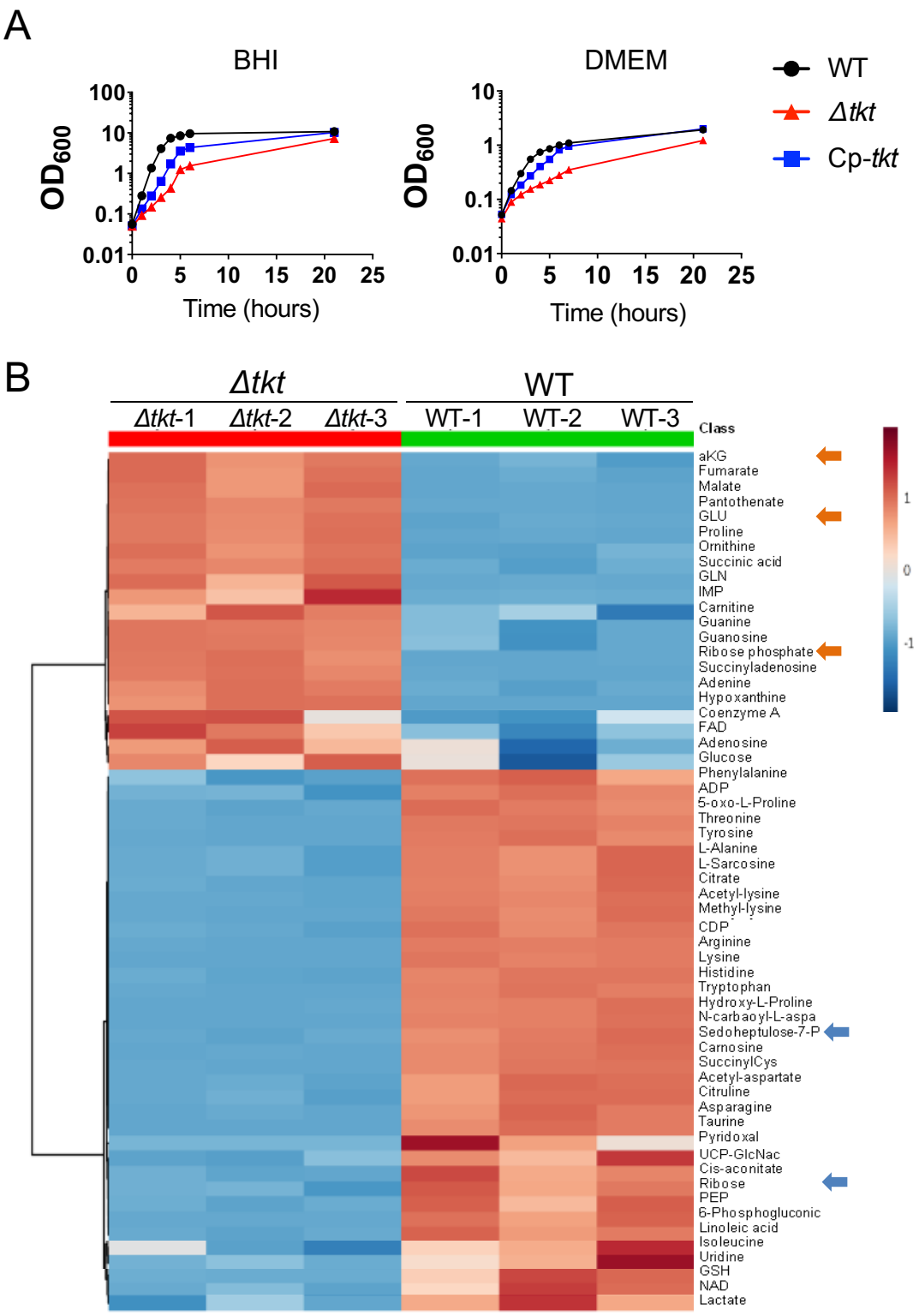
A
BHI
DMEM
WT
Δtkt
Cp-tkt
OD600
Time (hours)
B
Δtkt
WT
Δtkt-1
Δtkt-2
Δtkt-3
WT-1
WT-2
WT-3
Class
aKG
Fumarate
Malate
Pantothenate
GLU
Proline
Ornithine
Succinic acid
GLN
IMP
Carnitine
Guanine
Guanosine
Ribose phosphate
Succinyladenosine
Adenine
Hypoxanthine
Coenzyme A
FAD
Adenosine
Glucose
Phenylalanine
ADP
5-oxo-L-Proline
Threonine
Tyrosine
L-Alanine
L-Sarcosine
Citrate
Acetyl-lysine
Methyl-lysine
CDP
Arginine
Lysine
Histidine
Tryptophan
Hydroxy-L-Proline
N-carbaoyl-L-aspa
Sedoheptulose-7-P
Carnosine
SuccinylCys
Acetyl-aspartate
Citruline
Asparagine
Taurine
Pyridoxal
UCP-GlcNac
Cis-aconitate
Ribose
PEP
6-Phosphogluconic
Linoleic acid
Isoleucine
Uridine
GSH
NAD
Lactate

Figure 2

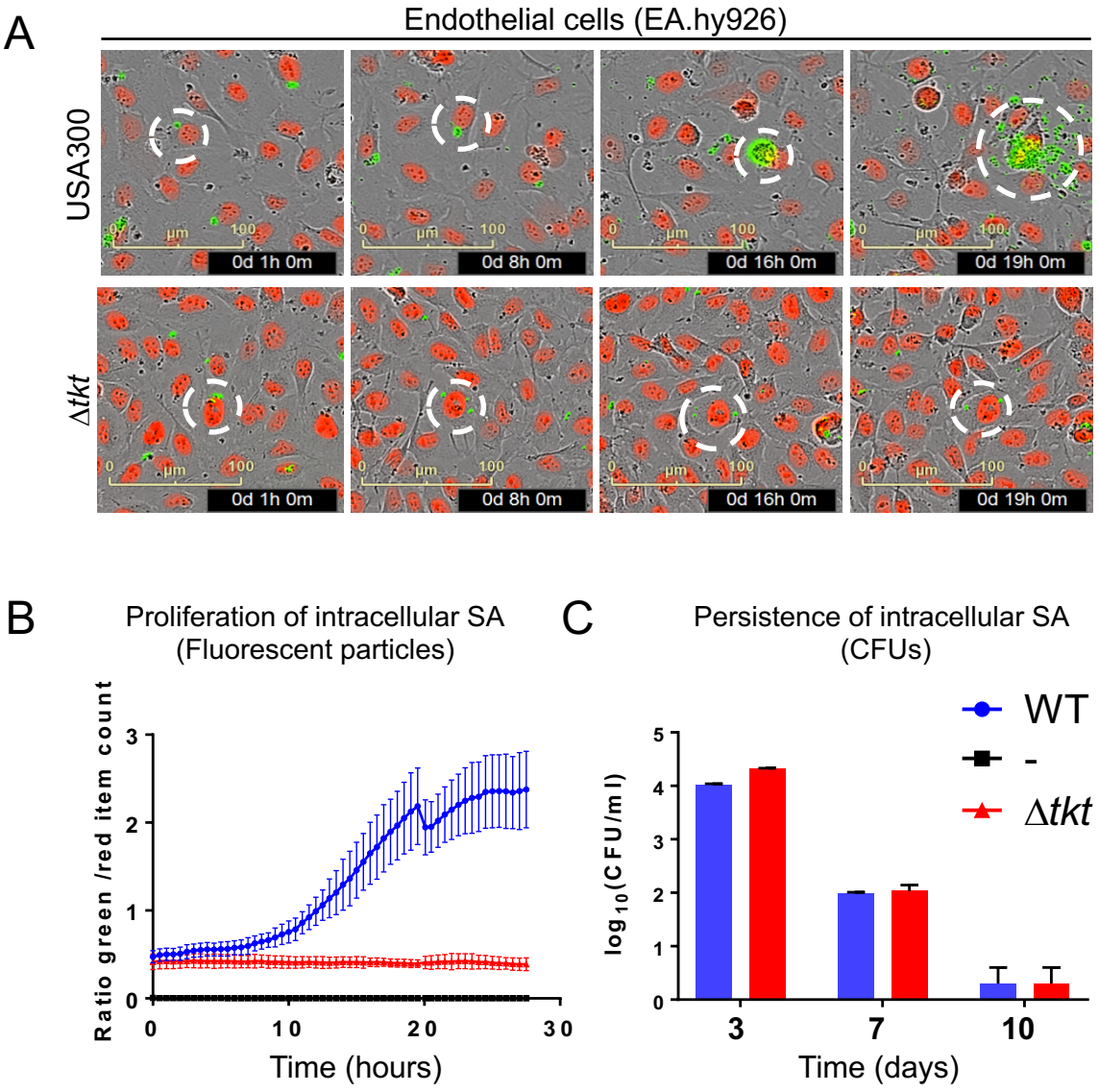
A
Endothelial cells (EA.hy926)
USA300
Δtkt
0d 1h 0m
0d 8h 0m
0d 16h 0m
0d 19h 0m
B
Proliferation of intracellular SA
(Fluorescent particles)
Ratio green /red item count
Time (hours)
C
Persistence of intracellular SA
(CFUs)
log10(CFU/ml)
Time (days)
WT
-
Δtkt

Figure 3

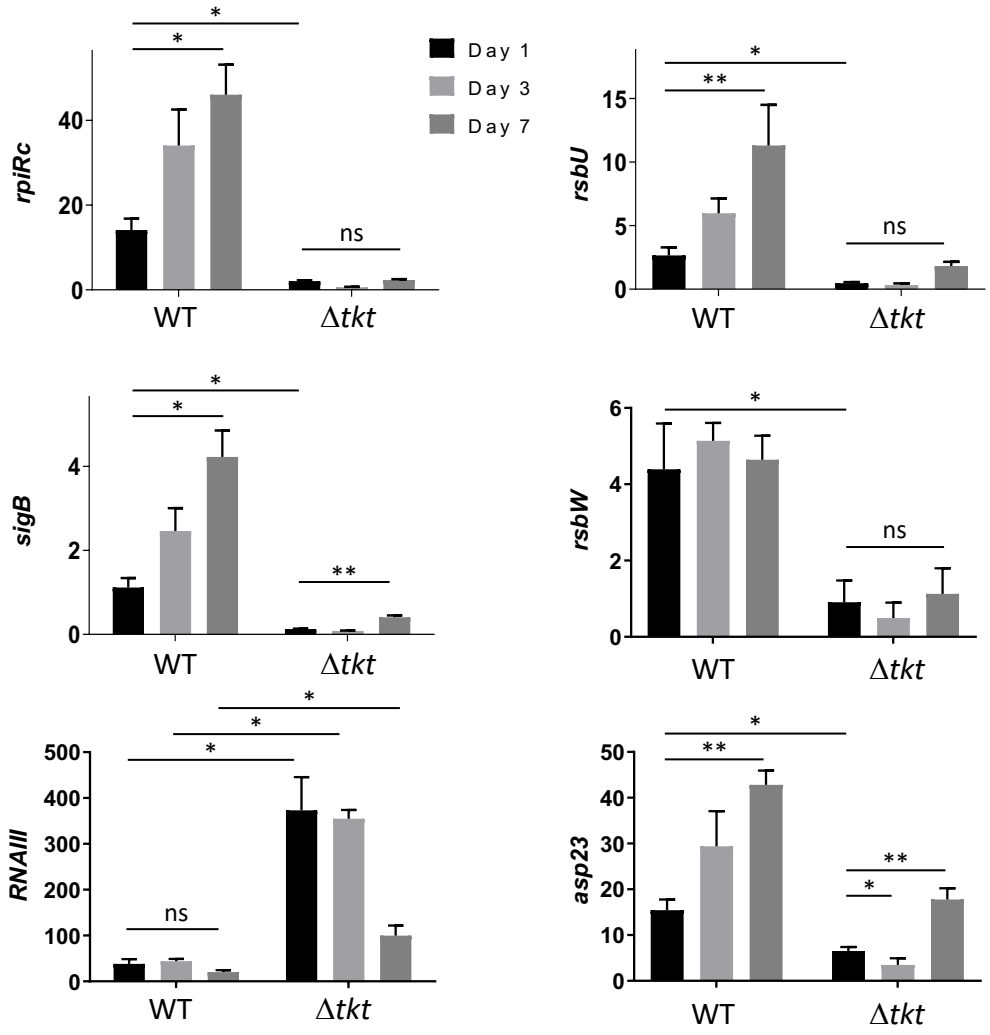

Figure 4

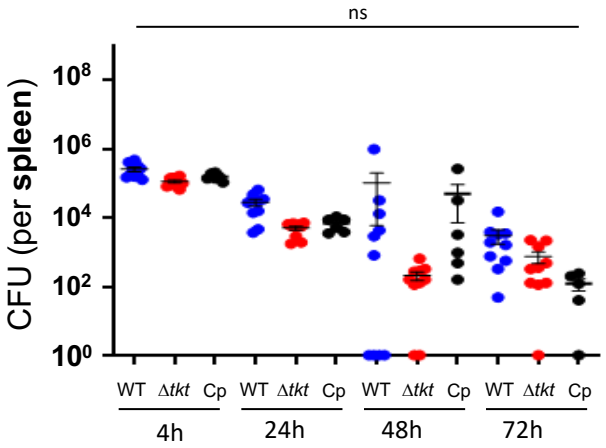
ns
CFU (per spleen)
10^8
10^6
10^4
10^2
10^0
WT Δtkt Cp WT Δtkt Cp WT Δtkt Cp WT Δtkt Cp
4h
24h
48h
72h

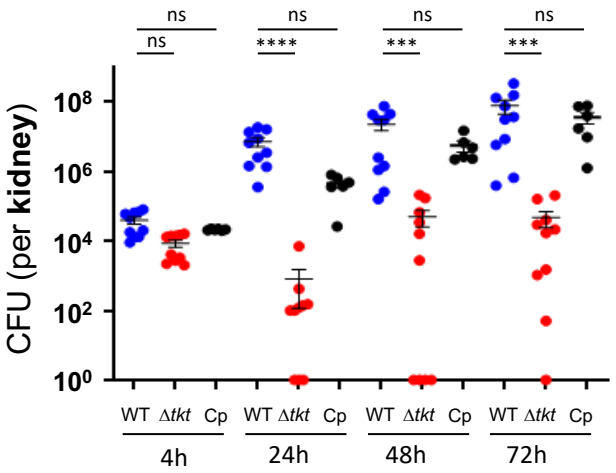
ns
ns
ns
ns
ns
****
***
***
CFU (per kidney)
10^8
10^6
10^4
10^2
10^0
WT Δtkt Cp WT Δtkt Cp WT Δtkt Cp WT Δtkt Cp
4h
24h
48h
72h

Figure 5

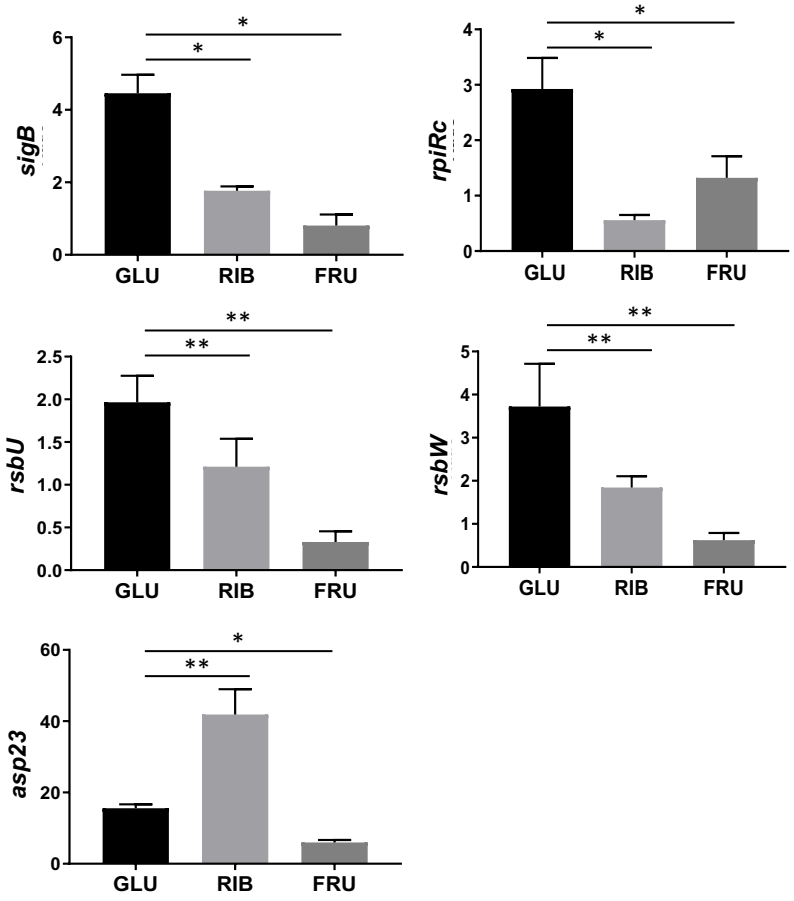

Figure 6

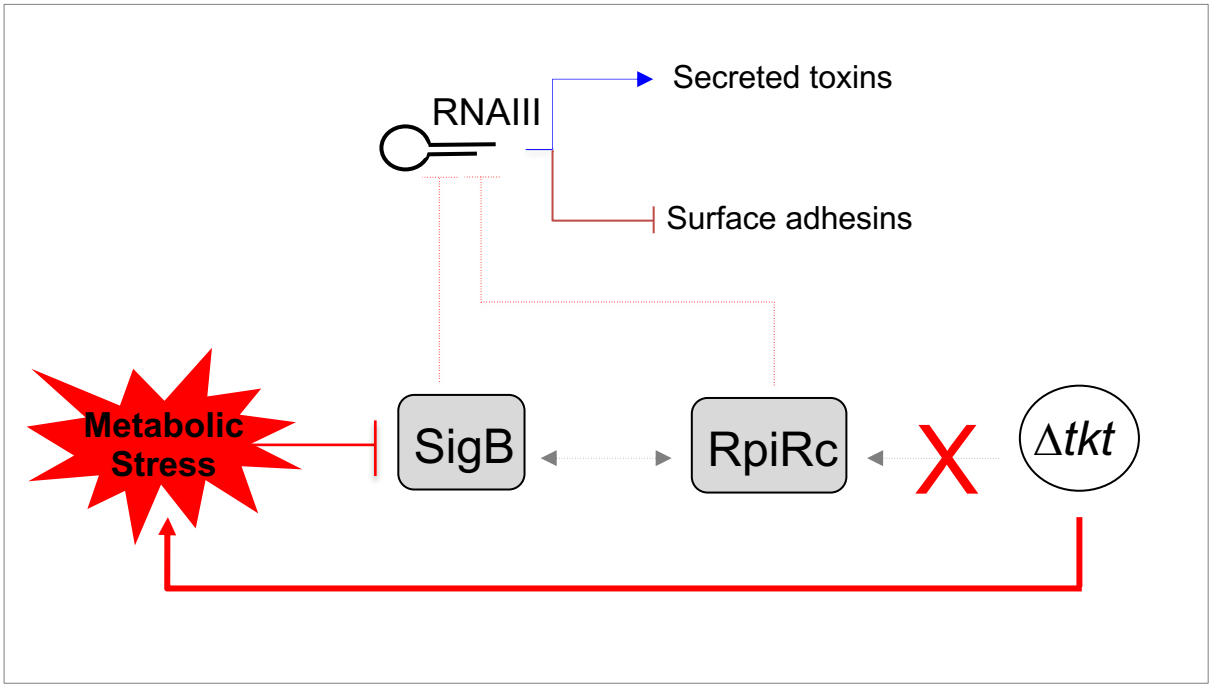
RNAIII
Secreted toxins
Surface adhesins
Metabolic Stress
SigB
RpiRc
X
Δtkt

Figure S1

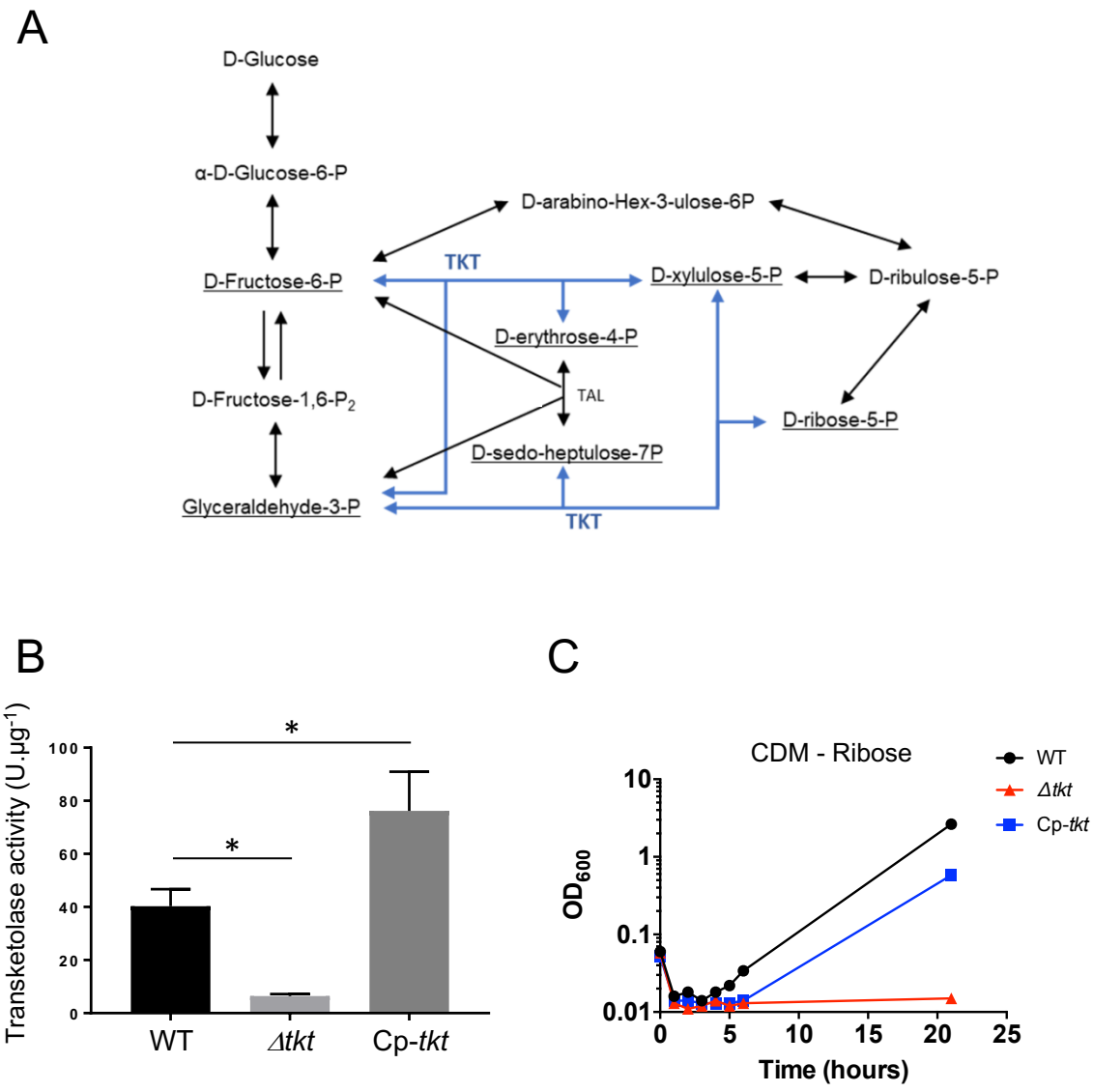

Figure S1. Characterization of the Δ*tkt* mutant strain.
A. Schematic depiction of the Pentose Phosphate Pathway. Light blue: TKT enzymatic reaction.
B. Transketolase activity. Transketolase activity was monitored in USA300 WT, Δ*tkt* and Cp-*tkt*. Inactivation of *tkt* gene led to a significant decrease in TKT enzyme activity (ANOVA: * p<0.001).
C. Growth of USA300 wild type (WT), Δ*tkt* mutant (Δ*tkt*) and its complemented derivative (Cp-*tkt*). USA300 WT, Δ*tkt* and Cp-*tkt* strains were grown in CDM supplemented with ribose as sole carbon source for 21 hours at 37°C. Optic densities were measured every-hour from 0 to 8 hours and then at 21 hours. Each panel is a representative experiment.

Figure S2

A

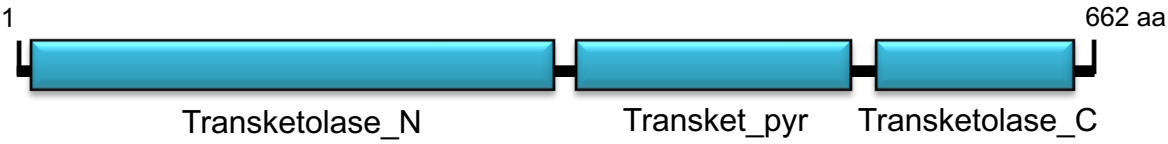

B

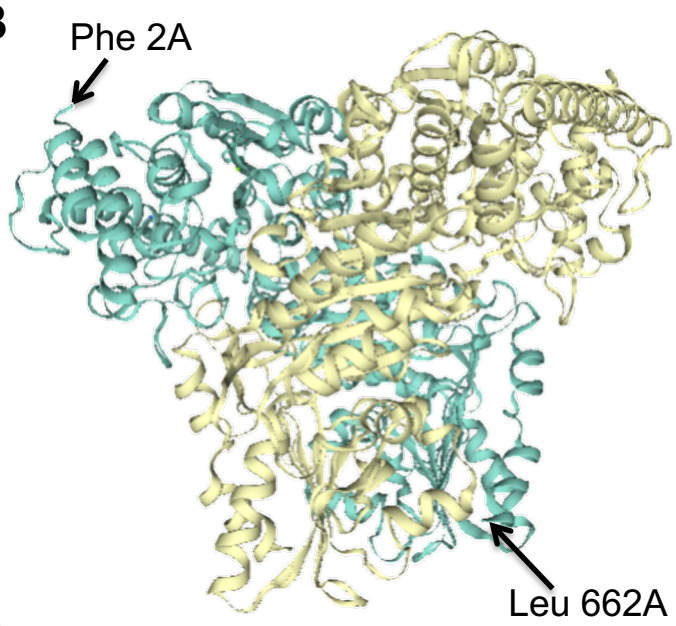

C

Protein ID	% coverage	% identity	Species
TKT_HUMAN	100.0%	100.0%	*Homo sapiens*
TKT_MOUSE	100.0%	94.7%	*Mus musculus*
TKT2_ECOLI	94.5%	24.1%	*Escherichia coli*
TKT_HAEIN	94.2%	22.9%	*Haemophilus influenzae*
TKT1_VIBCH	94.4%	24.0%	*Vibrio cholerae*
TKT_DICDI	94.2%	22.6%	*Dictyostelium discoideum*
TKT1_YEAST	94.5%	23.8%	*Saccharomyces cerevisiae*
TKT_TREPA	93.9%	21.9%	*Treponema pallidum*
TKT_MYCBO	96.6%	20.6%	*Mycobacterium bovis*
TKT_STRPN	94.2%	23.0%	*Streptococcus pneumoniae*
TKT_STAAS	94.4%	22.4%	*Staphylococcus aureus*
TKT_BACSU	94.9%	22.7%	*Bacillus subtilis*

Figure S2. Transketolase proteins domain organization and structure.

A. Conserved domains found in *S. aureus* transketolase. Transketolase_N (PF00456 domain): Transketolase, thiamine diphosphate binding domain; Transket_pyr (PF02779 domain): Transketolase, pyrimidine binding domain; Transketolase_C (PF02780): Transketolase, C-terminal domain (putative regulatory molecule binding site).

B. Protein model of *S. aureus* transketolase. Swiss-Model was used to predict the structure of *S. aureus* TKT (SAUSA300_1239) as a homodimer based on the template 3M49.1.A (Crystal Structure of Transketolase from *Bacillus anthracis*). The QMQE score and QMEAN were 0.83 and -0.59 respectively.

C. Table showing coverage percentage between transketolase amino acid sequences and percentage of identical amino acids between aligned transketolase amino acid sequences. Protein sequences were retrieved from UniProt database and aligned using Clustal Omega.

Figure S3

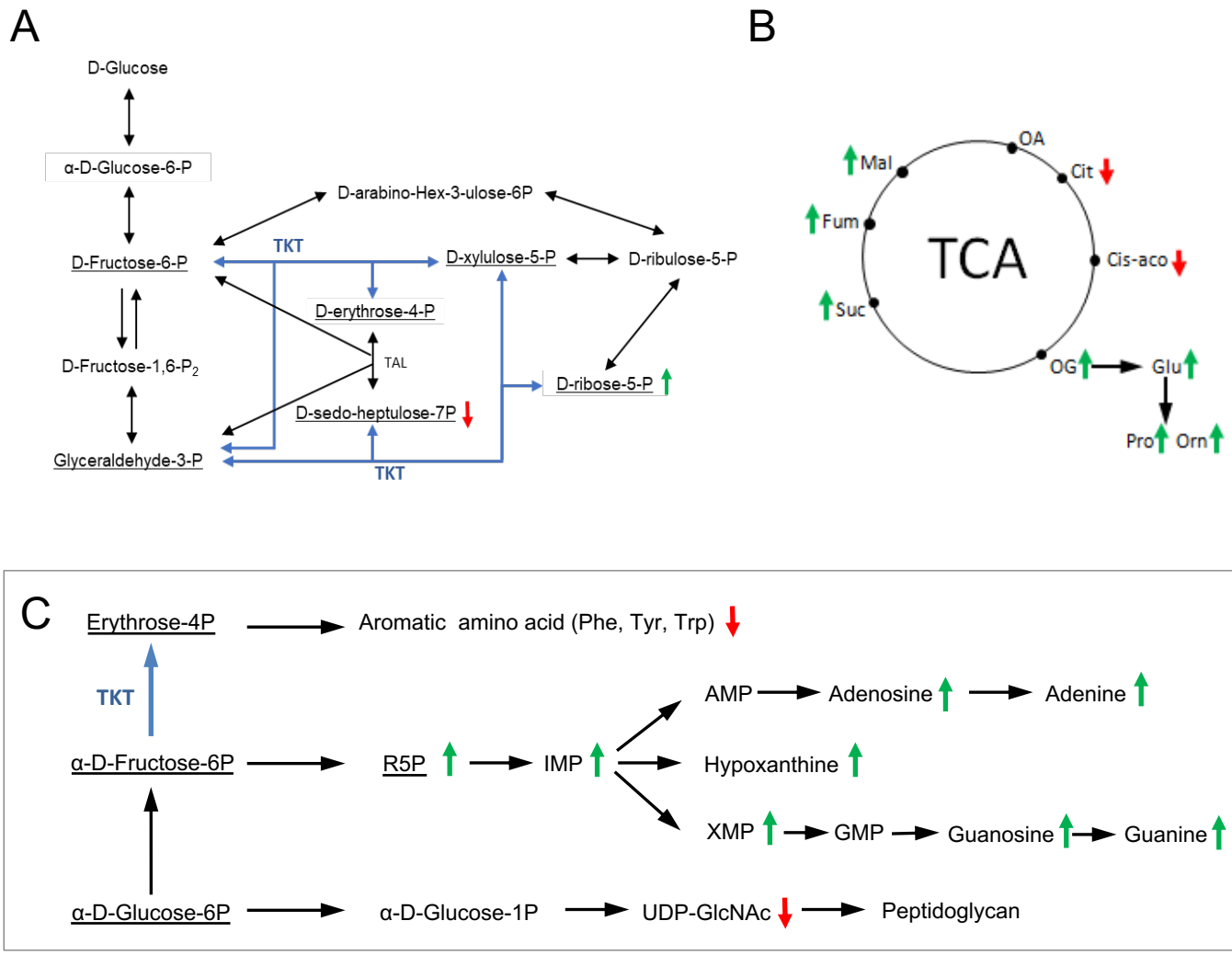

Figure S3. Metabolomic analysis of the Δ*tkt* mutant strain.
Quantitative metabolomic analysis was performed by ion chromatography and tandem mass spectrometry (IC-MS/MS) after overnight cultures, in BHI Broth, from WT USA300 and Δ*tkt* mutant strains (see **Table S1**). A, B and C. Highlight on metabolic pathways. Light blue: TKT enzymatic reaction. Green arrow: increased concentration in Δ*tkt* mutant compared to WT strain. Red arrow: decreased concentration in Δ*tkt* mutant compared to WT strain.

Figure S4

A

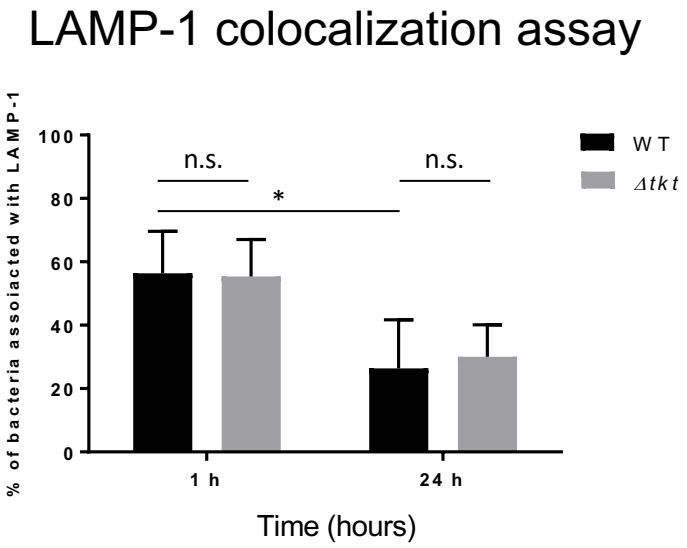

Figure S4. LAMP-1 colocalization assay

LAMP-1 colocalization assay. Endothelial EA.hy926 cells were infected with GFP-expressing WT and *Dtkt* mutant strains. One hour after infection, cells were washed several times with gentamicin containing medium to eliminate extracellular bacteria. A gentamicin concentration of 50µg/ml was maintained throughout the experiment. At 1 hour and 24 hours after infection cells were fixed using 4% PFA and processed for immunohistochemistry. Lysosomes were stained using anti-LAMP1 antibodies and images were acquired by confocal microscopy. Quantification of colocalization between GFP expressing USA300 WT or Δ*tkt* bacteria and LAMP-1 staining was obtained using ImageJ software. Data were obtained from more than 200 infected cells for each condition and expressed as % of bacteria associated with LAMP-1 ± SD. (ANOVA; n.s.: not statistically different; * $p<0.05$).

Figure S5

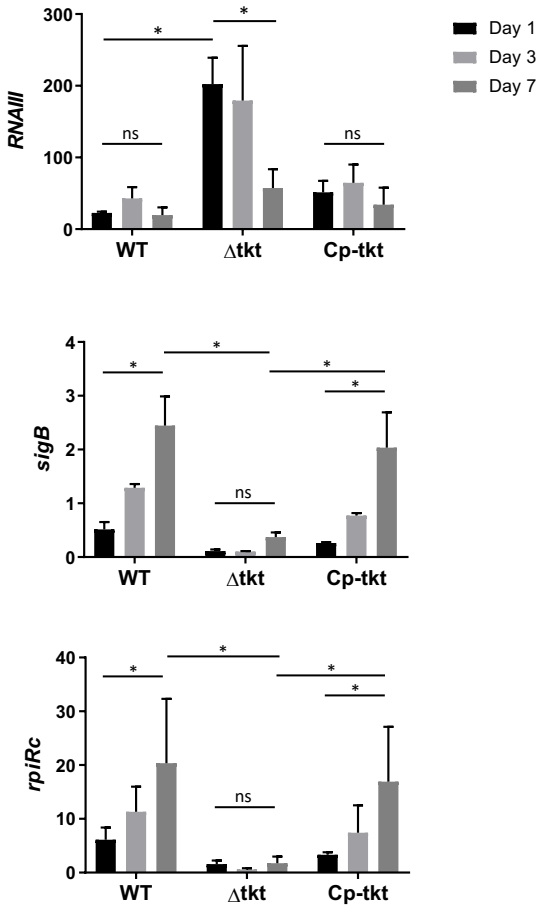

Figure S5. Transcription profile of intracellular *S. aureus*.
Endothelial EA.hy926 cells were infected with USA300 WT, Δ*tkt* and Cp-*tkt* strains as described in figure 2. One, three or seven days after infection cells were washed and collected. RNA from intracellular *S. aureus* were prepared and gene expression of *RNAIII*, *rpiRc* and *sigB* was analysed by quantitative RT-PCR. Gene expression level was normalized by that of *gyrA* at days 1, 3 and 7 after infection of EA-hy296 cells. Data are shown as mean normalized expression ± SD of triplicate measurements from two independent experiments. (ANOVA, ns : not statistically different; * $p<0.01$, ** $p<0.001$).
Experiments presented in Figure S5 were independent of those presented in Figure 3.

Supplementary Methods

Strains, Cells, Culture conditions and Infection.

S. aureus. The epidemic clone *S. aureus* USA300-LAC (designated USA300-WT) was provided by the Biodefense and Emerging Infections Research Resources (BEI). The GFP-expressing strain was generated by curing the p03 plasmid from USA300-WT and introducing the pCN57-GFP recombinant plasmid (obtained from the BEI) by electroporation as described before [1]. The Δ*tkt* mutant strain and the complemented strain were constructed as described below. Strains and plasmids used are summarized at the end of these supplementary methods.

Before experiments bacteria were grown 24 hours at 37°C on BHI agar plates supplemented with antibiotics when required and then overnight in BHI Broth from an optical density 600 nm (OD_{600}) of 0.05. The day of experiment, bacteria were resuspended in BHI broth to an OD_{600} of 0.05 and grown at 37°C until the culture reached the initial-middle log phase (OD_{600} of 0.6).

Growth curve were performed in brain heart infusion, DMEM and chemically defined medium (CDM) supplemented with ribose or fructose or glycerol when it was required [2].

Internalization rate and survival inside the EA.hy926 endothelial cell line were similar between the GFP strain and the parental strain.

Cell line. EA.hy926 cell line (ATCC CRL-2922), originally derived from human umbilical vein, were grown in Dulbecco's modified Eagle high glucose medium (DMEM, Dominique Dutscher) supplemented with 10 % fetal bovine serum (FBS, Thermofisher scientific) in a humidified 5 % CO_2 atmosphere at 37 °C. When indicated cells were incubated with no glucose DMEM supplemented with glucose, ribose or fructose at a concentration of 25mM. To facilitate cell identification and counting during time lapse experiments, EA.hy926 cells were transduced with the IncuCyte® NucLight Red Lentivirus, following the manufacturer's

recommendations, to obtain red nuclear labelling of living cells due to the expression of the red fluorescent protein mKate2 containing a nuclear localization signal.

Infection.

When fresh cultures reached OD_{600} of 0.6, bacteria were added to endothelial cells at a multiplicity of infection (MOI) of 1 and placed in a humidified 5 % CO_2 atmosphere at 37 °C for 1 h. One hour after infection, each well was washed three times with 100 µL of phosphate buffer saline (PBS) containing 300 µg/mL gentamicin, to remove extracellular bacteria. Cells were then incubated with 100 µL of cell culture medium containing 50 $\mu g.mL^{-1}$ gentamicin. Infected cells were kept in a humidified 5 % CO_2 atmosphere at 37 °C. Importantly, gentamicin is an antibiotic with a high bactericidal effect on *S. aureus* USA300 (CMI=2 $\mu g.mL^{-1}$) and a very poor penetration inside eukaryotic cells. In our model the use of gentamicin in the extracellular medium was necessary to abolish extracellular proliferation.

Construction of the *S. aureus* Δ*tkt* chromosomal deletion mutant

We inactivated the *tkt* gene in wild-type *S. aureus* USA300 strain and substituted it by the kanamycin resistance gene *npt*II fused with pG*ro* promoter. For this, we used the pMAD-temperature-sensitive shuttle vector system [3]. Briefly, the recombinant plasmid pMAD-Δ*tkt* was constructed by overlap PCR. First, the two regions (upstream 694bp, downstream 567bp) flanking *tkt* and the *npt*II gene (fused with pG*ro* promoter 1,091bp) were amplified by PCR. The region (2,352 bp) was then amplified by two-step overlap PCR. The resulting PCR product was cloned in pMiniT 2.0 (to yield recombinant plasmid pMiniT/tktUp-npt-tktDown). This recombinant plasmid was digested with *Bam*HI and *Eco*RI (New England BioLabs) and the *Bam*HI-*Eco*RI tktUp-npt-tktDown DNA fragment was finally subcloned into *Bam*HI-*Eco*RI-digested pMAD. All PCR reactions were realized using Phusion High-Fidelity DNA Polymerase (Thermofisher Scientific) and PCR products were purified using QIAquick PCR purification kit (Qiagen). The pMAD-Δ*tkt* plasmid was first introduced into *S. aureus* RN4220 prior to electroporation into *S. aureus* USA300. We used a standard two-step allelic

exchange procedure [3] to create the chromosomal *S. aureus* USA300 Δ*tkt* strain. The Δ*tkt* strain was finally checked for loss of the corresponding wild-type genes by PCR sequencing (Eurofins Genomics) using specific primers (described at the end of these supplementary methods).

Construction of the complementation of *S. aureus* Cp-*tkt* strain

The plasmid pCN57-CP*tkt* was constructed by homologous recombination [4]. The pCN57 linear vector and *tkt* gene fragments were amplified by PCR. To allow recombination, overlapping region of 20pb was added at each ends. PCN57 was linearized using SphI (New England BioLabs). *E. coli* DH5α were chemically transfected with a mix of both PCR product (insert: vector stoichiometry 2:1, 100ng of vector) in 10 µl MilliQ water. The colonies containing plasmid pCN57-CP-*tkt* were checked by PCR and the construct was sequenced. The pCN57-CP-*tkt* vector was then transfected into *S. aureus* RN4220 prior to electroporation into *S. aureus* USA300 Δ*tkt*. The Δ*tkt*-Cp-*tkt* (Cp-*tkt*) strain was finally checked for complementation of wild-type genes by PCR sequencing (Eurofins Genomics) using specific primers.

Time lapse microscopy

Four days prior to infection, NucLight Red labelled EA.hy926 cells were seeded in ImageLock 96-well plates (Essen BioScience Inc) in culture medium without antibiotic. Cells were infected with wild-type and mutant of the GFP-expressing USA300 strain as described above. Plates were incubated and monitored at 5% CO2 and 37°C for 24 hours in the fully automated microscope Incucyte® S3 (Essen BioScience). Images were taken every 30 minutes with the 20X objective. The medium was changed once during the observation period. Analysis and time-lapse videos (from which images were extracted) were generated by using Incucyte® S3 software.

Detailed analysis: Green items were analysed with a threshold of 1 GCU and using Top-hat segmentation mode. Red item were analysed with a threshold of 3 RCU and using Top-hat

segmentation mode and edge sensitivity of -25. A spectral unmixing of 10% was applied to remove red signal from green signal. Green item counts were considered as an approximation of the number of intracellular bacteria, and red item counts considered as the number of EA-hy296 cells. (Green items/Red items) represents the number of intracellular bacteria per cell during the time of infection.

Transcriptional analyses

Intracellular bacteria RNA extraction: EA.hy926 cells were grown to confluence in 75 cm^2 flasks and infected with *S. aureus* as described above. At selected time points, the culture medium was removed and the flasks were washed twice with PBS without antibiotics. Cells were lysed with 5 mL of distilled water for 10 min and the surface of the flask was scraped to detach the cells. The contents were recovered and centrifuged for 5 min at 3000 *g*. The supernatant was carefully removed and the pellet (which contained cell debris and bacteria) was resuspended in 100 µL of TE buffer containing 20 µg of lysostaphin and incubated for 5 minutes at 37 °C [5] to allow cell wall peptidoglycan degradation.

Planktonic bacteria RNA extraction: S. aureus was resuspended in CDM supplemented with glucose, ribose or fructose to an OD_{600} of 0.05 and grown overnight at 37°C. Bacteria were centrifuged at 12 000 *g* for 2 min and incubated in 50 µL of TE buffer containing 10 µg of lysostaphin for 5 minutes at 37 °C. The samples were resuspended in Trizol (Thermofisher Scientific) and treated with chloroform. RNAs were recovered using RNeasy Clean-up column (Qiagen) and DNA was digested using Turbo Dnase (Thermofisher Scientific). RNA concentration was measured using NanoDrop 1000 (Thermofisher Scientific). Reverse transcription was carried out with 500 ng of RNA and 0.5 µg of random primers (Promega). After denaturation at 70 °C for 5 min, 15 µL of the mix containing 4 µL M-MLV 5 X reaction buffer, 1 µL of 0.5 mM PCR Nucleotide Mix, 0.5 µL of RNasin Ribonuclease Inhibitor, and 1 µL M-MLV Reverse Transcriptase (Promega) was added. Samples were incubated 5 min at 25 °C, 1 h at 42 °C, then 15 min at 70 °C and chilled on ice. Quantitative RT-PCR was performed using FastStart SYBR Green qPCR Master Mix (ThermoFischer Scientific) or

Luna Universal qPCR Master Mix (New England Biolabs) according to the manufacturer's recommendations. Transcript levels were analyzed using a 7900HT Fast Real-Time PCR System (Applied Biosystems) according to the standard settings of the system software. The thermal cycling conditions were: 50°C for 2 min, 95°C for 10 min, followed by 40 cycles of 95°C for 15 s and 60°C for 1 min. Gene specific primer sequences are presented at the end of these supplementary methods. Expression of the gene *gyrA* was chosen as a reference. We used the "The Relative Standard Curve Method" for analyzing the qRT-PCR data.

Metabolomic analyses

Bacteria: Metabolite profiling of *S. aureus* isolates was performed by liquid chromatography–mass spectrometry (LC-MS) as described [6, 7]. Two independent experiments with three biological replicates were performed for each isolate. Briefly, *S. aureus* strains were grown in BHI Broth overnight to stationary phase and pelleted by centrifugation. Metabolic activity was blocked by immersion in liquid nitrogen for 10 sec. Metabolites were extracted using a solvent mixture of Methanol/ACN/H2O (50:30:20) at −20 °C (Extraction solution). Samples were vortexed for 5 min at 4°C, and then centrifuged at 16,000 g for 15 minutes at 4°C.

Endothelial cells: EA.hy926 endothelial cells were grown to confluence on a 12-well plate in no glucose DMEM supplemented with glucose or fructose or ribose (25 mM). One independent experiment with three biological replicates was performed for each condition. At each time points the cells were washed with cold PBS. Metabolism was blocked by plunging the plate into liquid nitrogen for 10 seconds. The cell metabolites were extracted from the samples by placing the cell culture plate on a rocking shaker at 4°C for 10 minutes. The extraction solution from each well was then collected and centrifuged at 16,000 g for 15 minutes at 4°C.

The supernatants were collected and analysed by LC-MS using SeQuant ZIC-pHilic column (Millipore) for the liquid chromatography separation [6]. The aqueous mobile-phase solvent was 20 mM ammonium carbonate plus 0.1% ammonium hydroxide solution and the organic mobile phase was acetonitrile. The metabolites were separated over a linear gradient from

80% organic to 80% aqueous phase for 15 min. The column temperature was 48 °C and the flow rate was 200 µl/min. The metabolites were detected across a mass range of 75–1,000 m/z using the Q-Exactive Plus mass spectrometer (Thermo) at a resolution of 35,000 (at 200 m/z) with electrospray ionization and polarity switching mode. Lock masses were used to insure mass accuracy below 5 ppm. The peak areas of different metabolites were determined using TraceFinder software (Thermo) using the exact mass of the singly charged ion and known retention time on the HPLC column. By this approach we were able to identify and measure: Glucose, Glucose-6P (G6P), UDP-glucose (UDP-Glc), Sedoheptulose-7-P (SH-7P), Ribose 5-phosphate, Glyceraldehyde 3-phosphate, Lactate, Pyruvate, Phospho-Enol-Pyruvate (PEP), Citrate (Cit), cis-aconitate (cis-aco), Succinate (Suc), Fumarate (Fum), Malate (Mal), alpha ketoglutarate (aKG), dihydroxyacetone phosphate (DHAP), N-carbamoyl-L-aspartate, Nicotinamide adenine dinucleotide (NAD), NADH, Nicotinamide adenine dinucleotide phosphate (NADP), NADPH, Adenine, Adenosine, Adenosine Mono, Di and Tri-phosphate (AMP, ADP, ATP), Cytidine, Cytidine Mono, Di and Tri-phosphate (CMP, CDP, CTP), Uridine Mono, Di and Tri-phosphate (UMP, UDP, UTP), Hypoxanthine, Guanine, Guanaosine, Guanidine Mono and Di-phosphate (GMP, GDP), Inosine monophosphate (IMP), Pantothenate, Dephospho-Coenzyme A, Coenzyme A (CoA), Flavin adenine dinucleotide (FAD), Niacin, Nicotinamide, 3-hydroxybutyrate, Urate, 5-oxo-L-Proline, Acetyl-aspartate, Acetyl-glutamine, Alanine, Arginine, Argininosuccinate, Asparagine, Aspartate, Betaine, Citrulline, Cystathionine, Cystine, Glutamine, Glutamate, Glycine, Histidine, IsoLeucine, Leicine, Sarcosine, Lysine, Methionine, Ornithine, Phenylalanine, Proline, Serine, Taurine, S-Adenosyl-L-methionine, Threonine, Tryptophan, Tyrosine, Valine, Butyric acid, Carnitine, Decanoic acid, Lauric acid, Hexanoic acid, Linoleic acid, Myristic acid, Octanoic acid, Oleic acid, Palmitic acid.

Statistical analyses were performed using MetaboAnalyst 4.0 software [8, 9]. The algorithm for heatmap clustering was based on the Pearson distance measure for similarity and the Ward linkage method for biotype clustering. Metabolites with similar abundance patterns were positioned closer together.

Transketolase activity assay

Bacteria were grown to stationary phase in BHI Broth and 1 ml of culture was harvested. Bacteria were washed in PBS, pelleted by centrifugation, and resuspended in 300 µl of 50 mM Tris with 60 µg lysostaphin, pH 7.5. Samples were incubated at 37 °C for 5 min and then sonicated at 4 °C (30s on, 30s off, repeated 30 times) (Diagenode). Samples were centrifuged at 12,000 *g* and 4 °C for 10 min to remove cell debris and protein concentration was determined using BCA assay with BSA as a standard (Thermo Fisher Scientific). TKT activity was analysed as described previously [10]. Briefly, each enzymatic reactions were performed at a final volume of 100 µl containing 20 µl of supernatant, 50 mM Tris (pH 7.5), 0.24 mM $MgCl_2$, 10 µM thiamine pyrophosphate, 0.5 mM NADH, 3 units of glycerol-3-phosphate dehydrogenase, 10 units of triosephosphate isomerase, 0.5mM D-xylulose-5-phosphate, and 0.5mM D-erythrose-4-phosphate (all reagents obtained from Sigma-Aldrich). The reaction proceeded at 37 °C for 5 min, and the decrease in $A_{340\ nm}$ was monitored with a microplate reader (Molecular Devices). Transketolase enzyme activity in bacteria lysates was expressed as units per microgram of total protein. One unit of enzyme was defined as the amount of enzyme that oxidized 1 µmol of NADH per minute.

LAMP-1 colocalization assay

EA.hy926 endothelial cells were grown to confluence on 8-well Slides (Lab Tek II) and infected with *S. aureus* as described above. For each point, cells were washed 3 times with PBS and fixed 20 min in PBS-4% paraformaldehyde at 4 °C. Fixation was stopped in PBS-NH_4Cl 50 mM. Cells were permeabilized with PBS containing 0.1% saponin and 5% goat serum for 10 min on ice. Cells were incubated for 30 min with anti-LAMP-1 (Lysosomal-associated membrane protein 1) rabbit polyclonal antibody (1/200e, AbCam) diluted in PBS containing 5% goat serum (staining buffer). After washing, cells were incubated for 30 min with Alexa-568 conjugated donkey anti-rabbit secondary antibodies (1/400e, AbCam) diluted in staining buffer. After washing, 4,6-diamidino-2-phenylindole (DAPI) was added (1/10,000e)

for 20 min and glass coverslips were mounted in Mowiol (Cityfluor Ltd.). Cells were examined using an X63 oil-immersion objective on an Apotome microscope (Zeiss^{TM}). Colocalization of GFP expressing bacteria with LAMP-1 staining was quantified by using Image J software (plug in: Coloc based Sur-vol _ Beta v6). Data were obtained from more than 200 infected cells for each condition and expressed as % of bacteria associated with LAMP-1 ± SD.

In vivo infection

For all experiments we used 6 to 10 weeks-old female BALB/c (Janvier Labs) with access to food and water ad libidum.

Infection. Overnight cultures of *S. aureus* in BHI Broth were diluted in BHI Broth to an OD_{600} of 0.05. Bacteria were grown at 37°C until the culture reached the initial-middle log phase (OD_{600}=0.6) and resuspended in a sterile isotonic saline solution to an OD_{600} of 0.4.

Mice were infected with 10^7 bacteria intravenously (iv) in the tail vein. Inoculum titers were checked by spreading dilutions of the preparations on BHI agar plates. For bacterial burden determination, mice were euthanized after 4, 24, 48 and 72 hours. Sequential dilutions of homogenized preparations from spleen and kidney were spread onto BHI agar plates.

Mice infected with the complemented strain were treated with erythromycin to avoid loss of the complementing plasmid. For this, mice received one dose of erythromycin 16 hours before infection and 2 doses of erythromycin per day until they were sacrificed (500 µg of erythromycin per dose).

Statistics

Data were analyzed using GraphPad Prism software. Results are presented either with one representative experiment for clarity or as means ± standard deviation (SD). The number of biological and technical replicates is indicated in the legend of each figure. For two-sample comparisons statistical significance was measured using unpaired two-tail Student's t-test. For comparisons between more than two groups, statistical significance was measured using

one-way analysis of variance (ANOVA) with Dunnett's correction. P values of $p<0.05$ were considered to indicate statistical significance.

Ethics statement

All experimental procedures involving animals were conducted in accordance with guidelines established by the French and European regulations for the care and use of laboratory animals (Decree 87–848, 2001–464, 2001–486 and 2001–131 and European Directive 2010/63/UE) and approved by the INSERM Ethics Committee (Authorization Number: 75-906).

Strains and plasmids used in this study.

Strain or plasmid	Relevant characteristic(s)	Source of reference
Strains		
E.coli		
DH5α	Φ80' *lacZ* ΔM15 *gyrA96 recA1 relA1 endA1 thi-1 hsdR17*	Invitrogen
S.aureus		
USA300 LAC	MRSA containing phage ΦSA2usa (PVL), Ery^R	BEI Resources
USA300-Ery^S	Erythromycin-sensitive derivative of USA300	Laboratory collection
RN4220	Restriction-deficient transformation recipient *S. aureus*	Laboratory collection
USA300 Δ*tkt*	*tkt* defective mutant, Kan^R	This study
USA300 Δ*tkt*-CP*tkt*	Complemented strain, USA300 Δ*tkt* containing pCN57-CP*tkt,* Ery^R Kan^R	This study
USA300 LAC-*gfp*	Strain containing pCN57-GFP, Ery^R	Laboratory collection
USA300 Δ*tkt-gfp*	USA300 Δ*tkt* containing pCN57, Ery^R Kan^R	This study
Plasmids		
pMAD	Plasmid with a thermosensitive origin, used for gene deletion; Amp^R Ery^R	Laboratory collection
pMAD-Δ*tkt*	Derivative of pMAD with upstream and downstream sequences from *tkt* gene and *nptII*[a], Amp^R Ery^R Kan^R	This study
pCN57	Plasmid containing *gfp* expression cassette (constitutive expression), Ery^R	Laboratory collection
pXT02	Derivative of pCN57. The *gfp*expression cassette was replaced by the sequence of the *tkt* gene with its own promoter.	This study

pMiniT 2.0	Plasmid used to clone upstream and downstream regions from *tkt* gene and *nptII,* Amp^R	New England Biolabs

[a]. *nptII*: neomycin phosphotransferase gene, determing kanamycin resistance.

Primers used for ∆tkt mutant construction and complementation

Primer name	Primer sequence (From 5' to 3')
tktup	F: CGGAATTCGAAGTAGGATTAACTCAAGAAGAAGC
	R: TTTAGCTCGACTAATCCATACAACTGCTAAAGCTAATCCTACTGAC
tktdn	F: CCTTCTTGACGAGTTCTTCTGAGGATGGCATAAATATGTAGGTACTG
	R: CGGGATCCATTTGCATCATCATCATACGAAGC
nptII	F: TTGTATGGATTAGTCGAGCTAAA
	R: TCAGAAGAACTCGTCAAGAAGG
s_tkt	F: GAATATCGAAAGAATTAACGAGTTAGC
	R: CGCACTCTTCATATTTTGATCCAT
s_pMAD	F: TCTGGCCATTGCTCTGGGTTA
	R: GCTGTCCCTGATGGTCGTCAT
HRtkt	F: CTTTGAGTGAGCTGGCGGCCGGATCCGGGTTTAAACAACAAATTGAAAATAC
	R: CATAGTAAGCTGCATGCAGCCCCGGGTTATAAGCTCATAACTTGGTTTAAGATATTTTC
HRpCN57	F: ACCAAGTTATGAGCTTATAACCCGGGGCTGCATGCAGCTTACTATG
	R: TCAATTTGTTGTTTAAACCCGGATCCGGCCGCCAGCTCACTCAAAG

Primers used for RT-qPCR.

Gene name	Primer sequence (From 5' to 3')
RNAIII	F: GCCATCCCAACTTAATAACCATGTAAAATTAGC
	R: GCGATGTTGTTTACGATAGCTTACATGCTAG
rpirC	F: CATACACGTACTACACGCGCACTTAATC
	R: GTCGGTAGCAACTACAAAAGATGCG
tkt	F: GGTCATAATGGTGCATCTCGTGC
	R: CATTGGATTTGTTTGAACCAGCAAGG
gyrA	F: GGTGGATTTGAAAACTTAGAGGACGAAGAC
	R: CATACCTTGAACACCACGACCACC
sigB	F: GGTGCCATAAATAGATTCGATATGTCCTT
	R: CTTTTGATTTCACCGATTACAGTAGGTACT
rsbU	F: CGCGTGAAGATGTGTTCAAGAC
	R: CTATCTCTTTATCGTGAACTTGAAG
rsbW	F: GAAGATTTTATCGAAATGCGC
	R: CATCATATGTAGCACCAGCTCTC

asp23	F: TCGCTGCACGTGAAGTTAAA
	R: CACCAACTTCAACAGATACACC

References

1. Rollin G, Tan X, Tros F, et al. Intracellular Survival of Staphylococcus aureus in Endothelial Cells: A Matter of Growth or Persistence. Frontiers in microbiology **2017**; 8:1354.

2. Hussain M, Hastings JG, White PJ. A chemically defined medium for slime production by coagulase-negative staphylococci. J Med Microbiol **1991**; 34:143-7.

3. Arnaud M, Chastanet A, Debarbouille M. New vector for efficient allelic replacement in naturally nontransformable, low-GC-content, gram-positive bacteria. Applied and environmental microbiology **2004**; 70:6887-91.

4. Jacobus AP, Gross J. Optimal cloning of PCR fragments by homologous recombination in Escherichia coli. PloS one **2015**; 10:e0119221.

5. Garzoni C, Francois P, Huyghe A, et al. A global view of Staphylococcus aureus whole genome expression upon internalization in human epithelial cells. BMC genomics **2007**; 8:171.

6. Mackay GM, Zheng L, van den Broek NJ, Gottlieb E. Analysis of Cell Metabolism Using LC-MS and Isotope Tracers. Methods in enzymology **2015**; 561:171-96.

7. TAN X, Coureuil M, Ramond E, et al. Chronic Staphylococcus aureus lung infection correlates with proteogenomic and metabolic adaptations leading to an increased intracellular persistence. bioRxiv **2018**.

8. Chong J, Soufan O, Li C, et al. MetaboAnalyst 4.0: towards more transparent and integrative metabolomics analysis. Nucleic acids research **2018**; 46:W486-W94.

9. Xia J, Wishart DS. Using MetaboAnalyst 3.0 for Comprehensive Metabolomics Data Analysis. Current protocols in bioinformatics **2016**; 55:14 0 1- 0 91.

10. Shaw JA, Henard CA, Liu L, Dieckman LM, Vazquez-Torres A, Bourret TJ. Salmonella enterica serovar Typhimurium has three transketolase enzymes contributing to the pentose phosphate pathway. The Journal of biological chemistry **2018**; 293:11271-82.

Figure S1

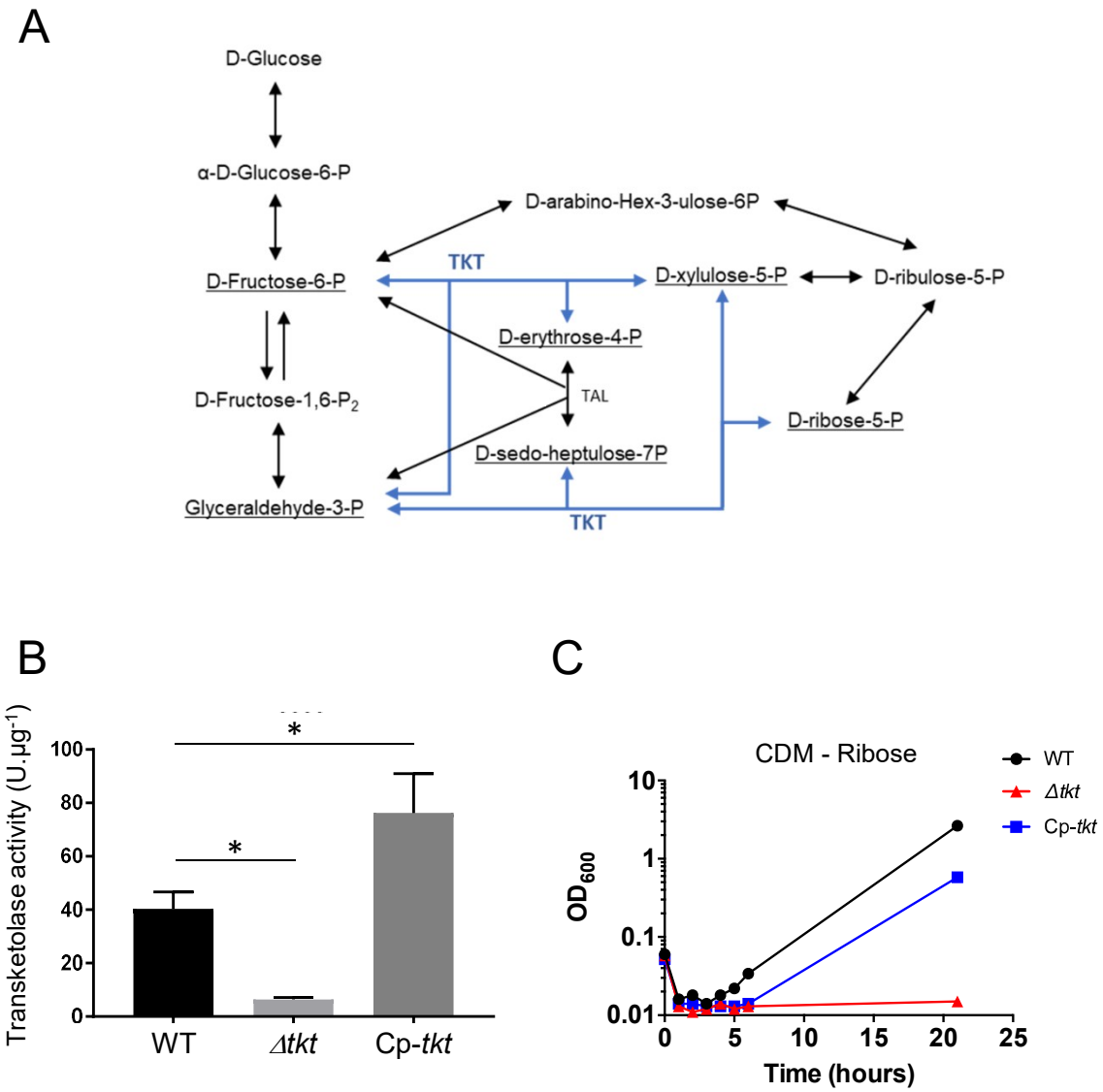

Figure S1. Characterization of the Δ*tkt* mutant strain.
A. Schematic depiction of the Pentose Phosphate Pathway. Light blue: TKT enzymatic reaction.
B. Transketolase activity. Transketolase activity was monitored in USA300 WT, Δ*tkt* and Cp-*tkt*. Inactivation of *tkt* gene led to a significant decrease in TKT enzyme activity (ANOVA: * p<0.001).
C. Growth of USA300 wild type (WT), Δ*tkt* mutant (Δ*tkt*) and its complemented derivative (Cp-*tkt*). USA300 WT, Δ*tkt* and Cp-*tkt* strains were grown in CDM supplemented with ribose as sole carbon source for 21 hours at 37°C. Optic densities were measured every-hour from 0 to 8 hours and then at 21 hours. Each panel is a representative experiment.

Figure S2

A

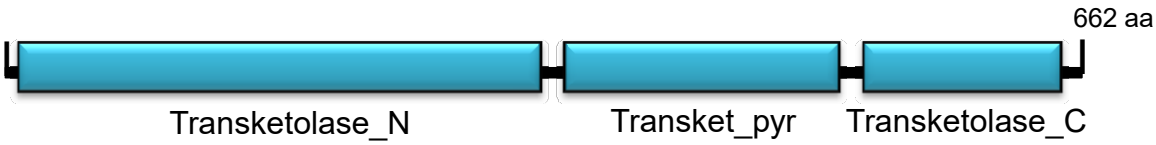

B

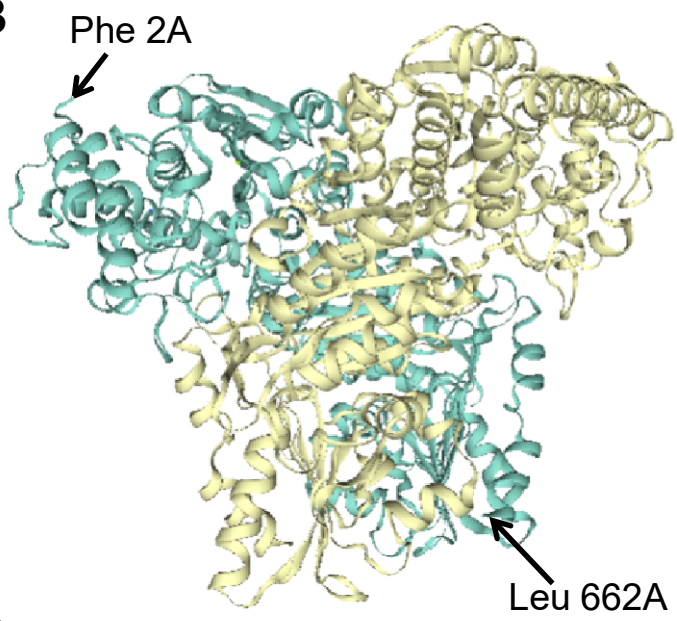

C

Protein ID	% coverage	% identity	Species
TKT_HUMAN	100.0%	100.0%	*Homo sapiens*
TKT_MOUSE	100.0%	94.7%	*Mus musculus*
TKT2_ECOLI	94.5%	24.1%	*Escherichia coli*
TKT_HAEIN	94.2%	22.9%	*Haemophilus influenzae*
TKT1_VIBCH	94.4%	24.0%	*Vibrio cholerae*
TKT_DICDI	94.2%	22.6%	*Dictyostelium discoideum*
TKT1_YEAST	94.5%	23.8%	*Saccharomyces cerevisiae*
TKT_TREPA	93.9%	21.9%	*Treponema pallidum*
TKT_MYCBO	96.6%	20.6%	*Mycobacterium bovis*
TKT_STRPN	94.2%	23.0%	*Streptococcus pneumoniae*
TKT_STAAS	94.4%	22.4%	*Staphylococcus aureus*
TKT_BACSU	94.9%	22.7%	*Bacillus subtilis*

Figure S2. Transketolase proteins domain organization and structure.
A. Conserved domains found in *S. aureus* transketolase. Transketolase_N (PF00456 domain): Transketolase, thiamine diphosphate binding domain; Transket_pyr (PF02779 domain): Transketolase, pyrimidine binding domain; Transketolase_C (PF02780): Transketolase, C-terminal domain (putative regulatory molecule binding site).
B. Protein model of *S. aureus* transketolase. Swiss-Model was used to predict the structure of *S. aureus* TKT (SAUSA300_1239) as a homodimer based on the template 3M49.1.A (Crystal Structure of Transketolase from *Bacillus anthracis*). The QMQE score and QMEAN were 0.83 and -0.59 respectively.
C. Table showing coverage percentage between transketolase amino acid sequences and percentage of identical amino acids between aligned transketolase amino acid sequences. Protein sequences were retrieved from UniProt database and aligned using Clustal Omega.

Figure S3

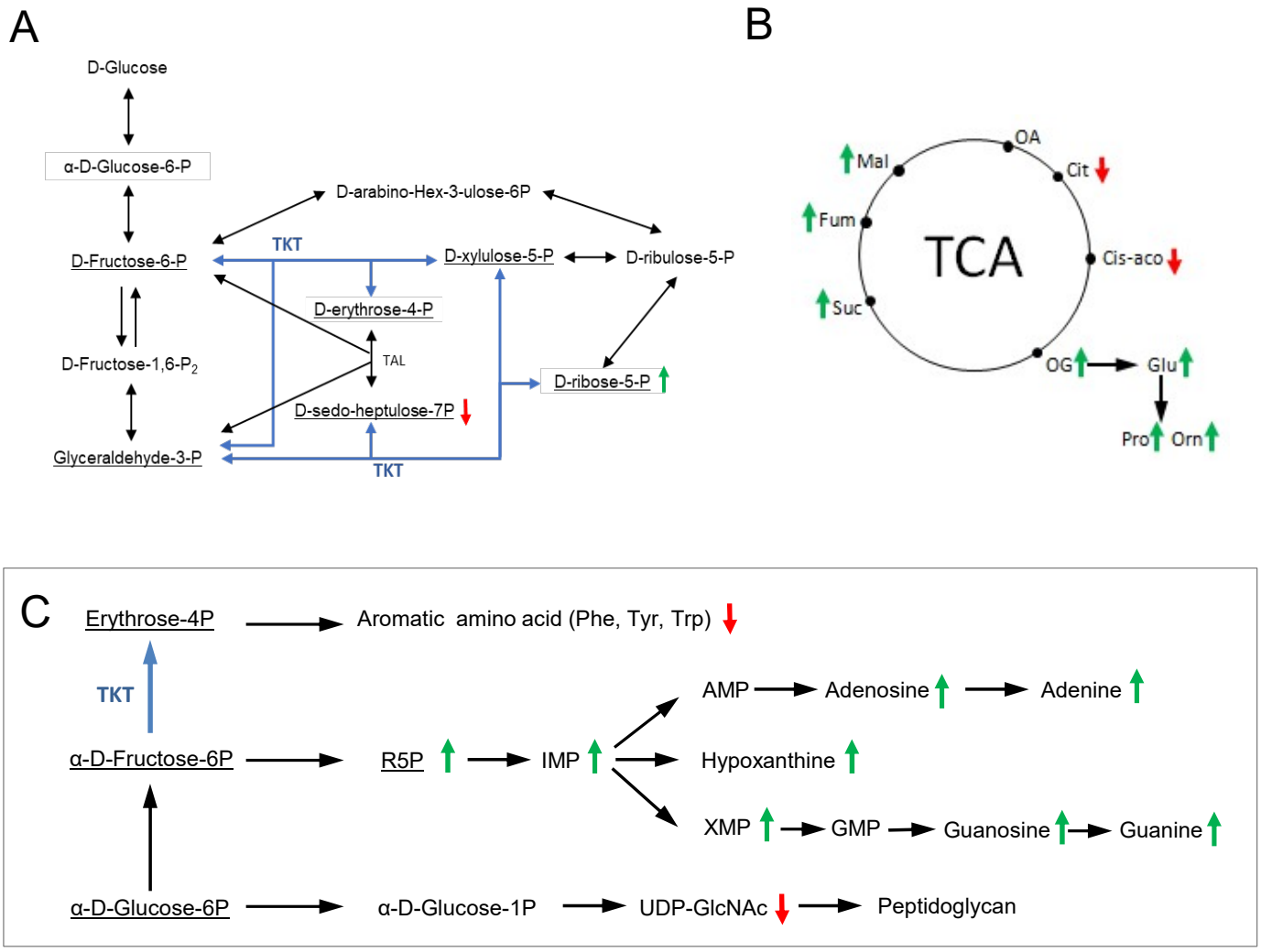

Figure S3. Metabolomic analysis of the Δ*tkt* mutant strain.
Quantitative metabolomic analysis was performed by ion chromatography and tandem mass spectrometry (IC-MS/MS) after overnight cultures, in BHI Broth, from WT USA300 and Δ*tkt* mutant strains (see **Table S1**). A, B and C. Highlight on metabolic pathways. Light blue: TKT enzymatic reaction. Green arrow: increased concentration in Δ*tkt* mutant compared to WT strain. Red arrow: decreased concentration in Δ*tkt* mutant compared to WT strain.

Figure S4

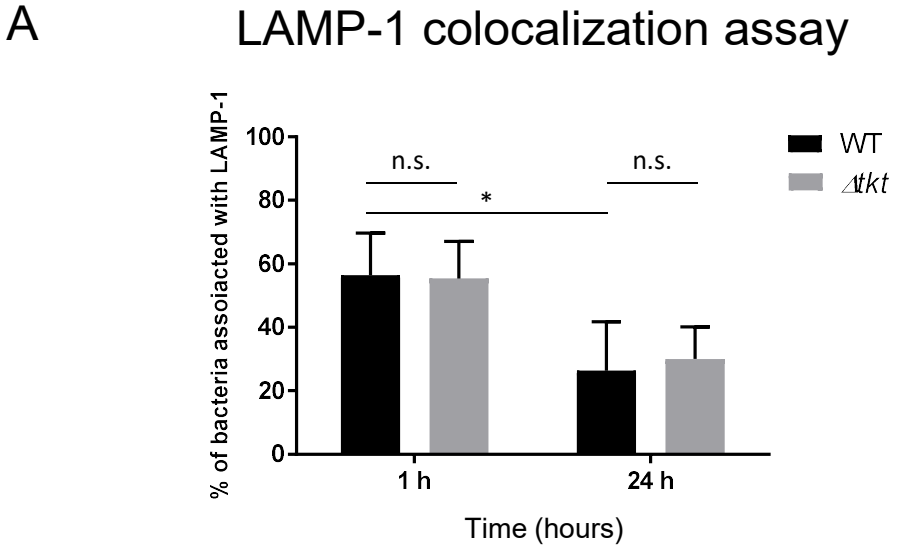

Figure S4. LAMP-1 colocalization assay

LAMP-1 colocalization assay. Endothelial EA.hy926 cells were infected with GFP-expressing WT and *Dtkt* mutant strains. One hour after infection, cells were washed several times with gentamicin containing medium to eliminate extracellular bacteria. A gentamicin concentration of 50µg/ml was maintained throughout the experiment. At 1 hour and 24 hours after infection cells were fixed using 4% PFA and processed for immunohistochemistry. Lysosomes were stained using anti-LAMP1 antibodies and images were acquired by confocal microscopy. Quantification of colocalization between GFP expressing USA300 WT or Δ*tkt* bacteria and LAMP-1 staining was obtained using ImageJ software. Data were obtained from more than 200 infected cells for each condition and expressed as % of bacteria associated with LAMP-1 ± SD. (ANOVA; n.s.: not statistically different; * $p<0.05$).

Figure S5

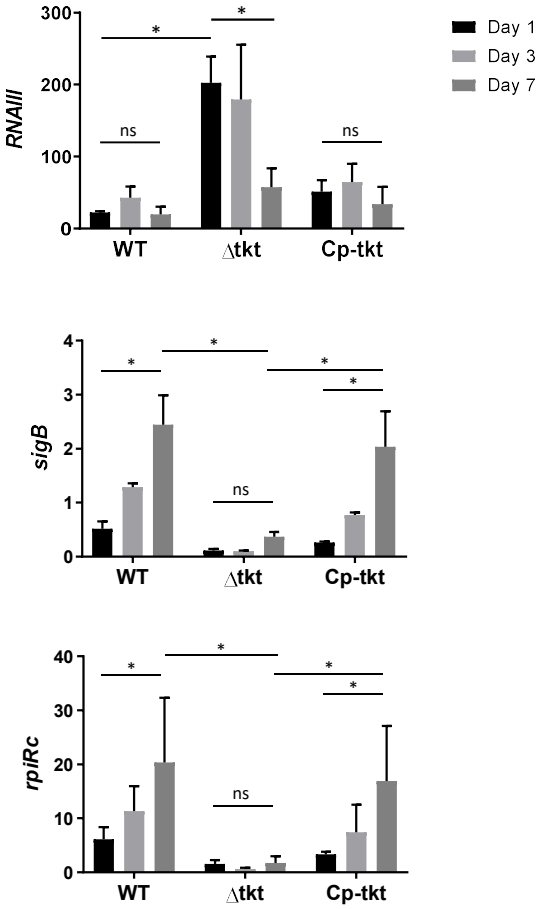

Figure S5. Transcription profile of intracellular *S. aureus*.
Endothelial EA.hy926 cells were infected with USA300 WT, Δ*tkt* and Cp-*tkt* strains as described in figure 2. One, three or seven days after infection cells were washed and collected. RNA from intracellular *S. aureus* were prepared and gene expression of *RNAIII*, *rpiRc* and *sigB* was analysed by quantitative RT-PCR. Gene expression level was normalized by that of *gyrA* at days 1, 3 and 7 after infection of EA-hy296 cells. Data are shown as mean normalized expression ± SD of triplicate measurements from two independent experiments. (ANOVA, ns : not statistically different; * p<0.01, ** p<0.001).
Experiments presented in Figure S5 were independent of those presented in Figure 3.